KfK 3556
Dezember 1983

Nuclear Densities of $1f_{7/2}$ Nuclei from Elastic Alpha-Particle Scattering

H. J. Gils, H. Rebel, E. Friedman
Institut für Kernphysik

Kernforschungszentrum Karlsruhe

KERNFORSCHUNGSZENTRUM KARLSRUHE

Institut für Kernphysik

KfK 3556

NUCLEAR DENSITIES OF $1f_{7/2}$ NUCLEI FROM ELASTIC ALPHA-PARTICLE SCATTERING

H.J. Gils, H. Rebel, E. Friedman[+)]

Kernforschungszentrum Karlsruhe GmbH, Karlsruhe

[+)] The Racah Institute of Physics
The Hebrew University of Jerusalem

Kernforschungszentrum Karlsruhe GmbH
ISSN 0303-4003

Abstract

The elastic scattering of 104 MeV α particles by $^{40,42,43,44,48}Ca$, ^{50}Ti, ^{51}V, ^{52}Cr has been analyzed by phenomenological and semi-microscopic optical potentials in order to get information on isotopic and isotonic differences of the α particle optical potentials and of nuclear matter densities. The phenomenological optical potentials based on a Fourier-Bessel description of the real part reveal different behavior in size and shape for the isotonic chain as compared to the isotopic chain. Odd-even effects are also indicated to be different for isotones and isotopes. The semi-microscopic analyses use a single-folding model with a density-dependent effective αN-interaction including a realistic local density approximation. The calculated potentials are fully consistent with the phenomenological ones. Isotopic and isotonic differences of the nuclear matter densities obtained from the folding model in general show a similar behavior as the optical potential differences. The results on matter densities are compared to other investigations.

KERNMATERIEDICHTEN VON KERNEN DER $1f_{7/2}$-SCHALE AUS ELASTISCHER α-TEILCHEN-STREUUNG

Zusammenfassung

Die elastische Streuung von 104 MeV α-Teilchen an $^{40,42,43,44,48}Ca$, ^{50}Ti, ^{51}V, ^{52}Cr wurde im Rahmen phänomenologischer und halb-mikroskopischer optischer Potentiale mit dem Ziel analysiert, Informationen über Differenzen der optischen Potentiale der α-Teilchen und der Kerndichteverteilungen der Isotopen- und Isotonenkette zu gewinnen. Die phänomenologischen optischen Potentiale basieren auf der Fourier-Bessel-Parametrisierung des Realteils, die ein unterschiedliches Verhalten der Isotopen- und Isotonenkette in Form, Stärke und Radius des Potentials offenlegt. Effekte zwischen Kernen mit gerader und ungerader Massenzahl (Ungerade-Gerade-Effekte) sind offenbar ebenfalls unterschiedlich bei Isotopen und Isotonen.

Die halb-mikroskopischen Analysen benutzen ein Faltungsmodell mit einer dichteabhängigen effektiven α-Nukleonwechselwirkung. Die berechneten mikroskopischen Potentiale sind vollkommen konsistent mit den phänomenologischen Potentialen. Die Unterschiede zwischen den Kernmaterieverteilungen der Isotopen- und Isotonenkette, die man aus den Faltungsmodellrechnungen erhält, sind im großen und ganzen ähnlich den Unterschieden zwischen den optischen Potentialen, zeigen jedoch im Detail interessante Abweichungen. Die Ergebnisse bezüglich der Kernmaterieverteilungen werden mit anderen Untersuchungen verglichen.

Content

Appendices

I. INTRODUCTION

One of the most conspicuous features observed with the $1f_{7/2}$ nuclei is the rather peculiar behavior of nuclear charge radii of the Ca-isotopes.[1-4] In the second half of the $1f_{7/2}$ neutron shell the charge radii decrease with increasing neutron number and they are almost equal for ^{40}Ca and ^{48}Ca. This trend is additionally superimposed by a distinct odd-even staggering. The charge radius of ^{43}Ca, for example, is considerably smaller than those of its neighbors. Obviously, it is quite interesting to look for the corresponding effects in matter and neutron distributions which are considered to be the origin of this rearrangement of the protons.[1,5-7] In addition, it is of great interest to see how matter and neutron distributions respond when protons are being added in an isotonic series. The experimental study of these questions is the subject of the present work which attempts to determine the differences of nuclear matter distributions of $1f_{7/2}$ isotones and isotopes including two odd mass nuclei (^{43}Ca, ^{51}V).

Unlike the case of the charge, studies of the distribution of neutrons in nuclei must inevitably rely on the use of strongly interacting probes, which introduces additional uncertainties into the analyses. In recent years, however, there has been considerable progress in understanding and handling these problems[1,5,6,8-13] and isotonic and isotopic variations are expected to be determined fairly reliably at least for series of neighboring nuclei. The present work is based on the elastic scattering of 104 MeV α particles by $^{40,42,43,44,48}Ca$ and by ^{50}Ti, ^{51}V, ^{52}Cr. The experimental results are characterized by an exceptionally wide angular range which enables to determine uniquely the optical potentials. The data for the even Ca isotopes has been analyzed before except that the experimental results for $^{40,48}Ca$ have slightly been extended and improved. A preliminary analysis of the experimental results for ^{50}Ti and ^{52}Cr, used in another context, has been published elsewhere.[14] The data for the odd nuclei ^{43}Ca and ^{51}V has not been published before.

The analysis in the present work has been significantly modified with respect to the accuracy of the radial moments of the real optical potentials and of the nuclear density distributions, which is of particular importance for the problem under consideration. In addition, the microscopic reaction model (single-folding model with density-dependent αN-interaction) used for the comparison of nuclear densities has considerably been improved [11,12] leading to full consistency with phenomenological descriptions.

The analysis in this paper is divided into two: in the first part we analyze the isotopic and isotonic variations of the real part of the optical potential. Although this potential is not simply related to nuclear densities it is, nevertheless, the quantity best determined [15] by experiment and it is expected to display isotopic and isotonic effects. In the second part we analyze the variations of the nuclear density distributions obtained within the folding model approach [5,12] to the optical potential.

Section II presents the method and in particular the new refinements introduced in this work. Section III presents the results and in Sec. IV these results are discussed.

II. METHOD

The method employed in the present work is similar to that used before [5,13-15] to analyze part of the same data but it has been refined in several ways which improve significantly the accuracy of information on isotopic and isotonic effects and on nuclear sizes derived from the same experimental data. In the case of the real part of the optical potential the accuracy of the radial moments is improved by introducing hitherto ignored correlations into the analysis of errors. In the case of the folding model, the modifications are three. First, a Gaussian plus Yukawa form factor is replacing the Gaussian interaction used previously.[5,11] Second, the Local Density Approximation (LDA) used in the density-dependent term of the effective

interaction has been modified[12] so that there is now better overall consistency and better fits to the data are achieved. Third, the ratios of radial moments of the nuclear matter density distribution and of the potential have been found to be extremely stable against variations in the numerical procedures and are therefore used as an additional method to calculate radial moments of the nuclear density distribution.

A. Optical potential analyses

The real part of the optical potential is written [13-16] as a sum of an initial approximation (usually a square of the conventional Woods-Saxon (WS) function) and a Fourier-Bessel (FB) series whose coefficients are obtained from a χ^2 minimization procedure:

$$- \text{Re } U(r) = V_o(r) + \sum_{n=1}^{N} b_n \, j_o \left(\frac{n\pi r}{R_c} \right). \qquad (1)$$

The imaginary potential is of the WS shape. This formulation has been shown [13-16] to lead to very good fits to the data and to realistic estimates of errors, both for the potential as a function of position r and for integral quantities of the potential such as its volume integral and various radial moments. The information about the uncertainties [15-17] is contained in the elements of a matrix (C) defined as

$$C_{mn} = \langle \Delta b_m \, \Delta b_n \rangle = 2 \, (M^{-1})_{mn} \, \chi^2/F \qquad (2)$$

where $\langle \Delta b_m \, \Delta b_n \rangle$ are the correlated uncertainties in the coefficients of the potential, (M) is the covariance matrix obtained numerically in the χ^2 fit and χ^2/F is the best value of χ^2 per degree of freedom obtained in the fit. With the elements of (C) one can evaluate the uncertainties of any quantity derived from the real potential. For example, the uncertainty of the real potential at a point r is given by

$$[\Delta \text{Re } U(r)]^2 = \sum_{m,n=1}^{N} C_{mn} \, j_o\left(\frac{n\pi r}{R_c}\right) \, j_o\left(\frac{m\pi r}{R_c}\right). \qquad (3)$$

The new feature in the present analysis is the reduced errors in the radial moments of the potential. These moments are defined as

$$M_k = \left[\frac{1}{J} \langle Jr^k \rangle \right]^{1/k} \tag{4}$$

where J is the volume integral of the real potential and

$$\langle Jr^k \rangle = \int \mathrm{Re}\ U(r)\ r^k\ d\vec{r}\,. \tag{5}$$

In evaluating the uncertainties in M_k we note that M_k is a ratio of two integrals, both containing Re U(r). As a result of correlations between the numerator and the denominator (also calculated with the help of (C)) there is a negative contribution to the errors of the radial moments which now read

$$\left[\frac{\Delta M_k}{M_k}\right]^2 = \left[\frac{\Delta \langle Jr^k \rangle}{\langle Jr^k \rangle}\right]^2 + \left[\frac{\Delta J}{J}\right]^2 - 2\frac{\overline{\Delta \langle Jr^k \rangle \cdot \Delta J}}{\langle Jr^k \rangle\ J} \tag{6}$$

where the last term represents these correlations. The first two terms in (6) are calculated as before.[16,17] When the full expression (6) is used, it is found that the errors in the radial moments are typically less than 50 % of the values obtained before [13, 15-17], which is an important feature in studies of differences between neighboring nuclei. The differences between the potentials themselves are also discussed in the present work and their uncertainties are obtained from eq. (3).

B. Folding model analyses

In the folding model approach one assumes [5,18,19] that the real part of the optical potential is given by folding an effective α-nucleon interaction into the density distribution of the

target nucleus:

$$- \text{Re } U(r) = \int V_{\alpha N}(\vec{r},\vec{r}',\rho_m)\ \rho_m(\vec{r}')\ d\vec{r}' \qquad (7)$$

where $\rho_m(\vec{r}')$ is the target nuclear matter density (point nucleons) normalized to the number of nucleons A. In previous analyses it was shown [5] that the effective interaction must be density - dependent if one is to fit data extending to large scattering angles. We therefore write [5,20]

$$V_{\alpha N}(\vec{r},\vec{r}',\rho_m) = f_{\alpha N}(|\vec{r}-\vec{r}'|) \cdot v_{DD}(\rho_m) \qquad (8)$$

where $f_{\alpha N}(|\vec{r}-\vec{r}'|)$ is the radial form factor of the (density-independent part of the) effective α-N-interaction, depending only on the distance $\vec{x} = |\vec{r}-\vec{r}'|$ between the α particle and the interacting nucleon. The second term $v_{DD}(\rho_m)$ parametrizes the density dependence of the interaction (see below). The form factor $f_{\alpha N}(\vec{x})$ is chosen to be a sum of a Gaussian and a Yukawa interactions [11],

$$f_{\alpha N}(\vec{x}) = V_G \exp[-|\vec{x}|^2/a_G^2] + V_Y \exp[-|\vec{x}|/a_Y]/(|\vec{x}|/a_Y). \qquad (9)$$

In the previous work [5] we used a Gaussian form factor which yielded, for all studied nuclei, systematically too small values for the various integral moments of the folding potentials as compared to the phenomenological ones.[5,15] The introduction of the additional Yukawa term mainly increases the long range tail of the effective interaction and thereby removes these discrepancies.

The density-dependent term of the effective interaction (8) is also modified now as compared to the previous work [5] where we wrote

$$v_{DD}^{T}(\rho_m) = \lambda \cdot [\ 1 - \gamma \rho_m^{2/3}(\vec{r}')\ ] \qquad (10)$$

with the normalization factor λ usually taken to be $\lambda = 1$.

This parametrization was originally found for the density-dependence of an effective nucleon-nucleon interaction [21,22] and was successfully applied also to αN-interactions using

the same value of the parameter $\gamma \approx 2$ fm^2. [5] The density dependence (11) was derived in the Brueckner-Hartree-Fock approximation for the interaction potential of a probe nucleon embedded in infinite nuclear matter of density ρ_m^o. For finite nuclei there is no à priori preference which density has to be inserted into (10) in a Local Density Approximation (LDA). One usually takes the density at the position of the one $\rho_m(\vec{r}_1)$ [21] or of the other $\rho_m(\vec{r}_2)$ interacting nucleons or the density in the middle between the two $\rho_m((\vec{r}_1+\vec{r}_2)/2)$ [10,23-25] or even some average density. For short range NN-interactions it is assumed [21] that these different choices of the LDA are equivalent. In the previous work we accepted this assumption (like others [25]) also for the αN-interaction and therefore inserted the density at the position of the interacting target nucleon $\rho_m(\vec{r}')$ into eq. (10). (The superscript T (target) in eq. (10) accounts for this particular choice). In a recent systematic analysis of different LDA choices, however, it has been shown [12] that an LDA of the form

$$v_{DD}^{M}(\rho_m) = \lambda \cdot [1-n\cdot\gamma\cdot\rho_m^{2/3}(\vec{r}')]\ [1-(1-n)\cdot\gamma\cdot\rho_m^{2/3}(\vec{r})] \qquad (11)$$

yields much better results in single-folding model analyses with a density-dependent αN-interaction. Here, $\rho_m(\vec{r}')$ is the target matter density at the position of the interacting target nucleon under consideration (as before) and $\rho_m(\vec{r})$ is the target matter density at the position of the α particle. With this form, in particular, a large degree of decoupling between the density-dependent and density-independent parts of the effective interaction is achieved (eq. (9) and (11)) thus supporting the factorization hypothesis (eq. (8)). The mixing parameter n ($0 \leq n \leq 1$) allows a continuous change of weighing the two factors. For n = 1 we have the previous form (eq.10) with the full weight on the position of the target nucleon. For n = 0, on the other hand, $v_{DD}(\rho_m)$ depends only on the density at the position of the α particle. We refer to this approach as a "mixed" (superscript M) local density approximation.

One of the main reasons for the preference of the "mixed" LDA (12) as compared to the form (10) arises from the fact that the dominant sources of the density dependence are Pauli forbidden intermediate states in the Brueckner reaction matrix and knock-on exchange terms of the Fock type. [26] Both contributions can not be independent of the density at the position of the probe α particle $\rho_m(\vec{r})$ (as assumed in eq. 10) and because of the long range of $f_{\alpha N}(\vec{x})$ this density cannot be replaced by $\rho_m(\vec{r}')$. Therefore, in eq. (12) the LDA is treated in an equivalent form for both interacting particles. The mixing parameter n has been phenomenologically determined to have the value n=0.2.[12] One can speculate that this value weighing the two factors in eq. (11) by the ratio 1 : 4 is related to the nucleon numbers of the interacting particles. We prefer, however, not to stress this parametrization and its parameter values too much and assume this agreement to be accidental. A more detailed justification of the improved LDA and a comparison with other approaches is given elsewhere.[12]

It should be emphasized that the effective interaction eqs. (8), (9), (11) need not be regarded as a fundamental one but only as a means of relating optical potentials to nuclear densities which hopefully is quite reliable at least over a limited range of nuclei. The parameters of the effective interaction V_G, a_G, V_Y, a_Y, and γ were obtained in a "calibration" procedure from a fit to the elastic α particle scattering cross sections from a nucleus whose density distribution ρ_m is assumed to be known. ^{40}Ca was chosen for this purpose and we used ρ_m calculated by Brown et al. [27] whose calculations reproduce very well the experimentally determined charge distribution of ^{40}Ca [28] and the result of Hartree-Fock calculations for the neutron density distribution. [29-31] (In the previous work [5] we used phenomenological $\rho_m(\vec{r})$). However, in this calibration procedure the parameters of $f_{\alpha N}(\vec{x})$ (eq.9) are not uniquely determined and, therefore, we fixed the value of a_Y during the fit. The value of a_Y was chosen in such a way, that the root-mean-square (rms) radius of the folded optical potential (eq. 7) reproduced the phenomenological value (obtained from the FB-potential fit, see Sect. III). The final parameter values are

V_G = 20.6 ± 0.6 MeV

a_G = 2.009 ± 0.006 fm

V_Y = 111. ± 2. MeV

a_Y = 0.85 fm

γ = 1.65 ± 0.02 fm²

n = 0.2

The improved effective αN-interaction (8), (9), (11) with the above parameter values leads to a very good agreement between the microscopic (folding) potential and the "model-independent" phenomenological FB-potential (see Sect. III). Moreover, also the goodness of fit of the folding model,expressed by the value of $\chi^2/F=2.6$,closely approaches the best value attainable by the FB-potential fit of $\chi^2/F=2.2$. These results are the justification for the modified procedures (in particular since they are also valid for the other nuclei). In spite of the continuous ambiguity between certain pairs of parameters the different new terms mainly influence different features of the folded potential so that it is not possible to obtain similarly good results when omitting one of the improvements introduced in the present work.

Once the effective αN-interaction had been chosen as described above the elastic scattering cross sections of all target nuclei under investigation including ^{40}Ca were fitted by varying the imaginary potential and parameters of $\rho_m(r)$. From ρ_m so obtained one could extract differences of nuclear matter densities and their corresponding radial moments. Although the procedures used were in general the same as in the previous work [5] we present and emphasize here some details which are important for the justification of the procedure and for the reliability of the results. We first describe the general method and then return to the particular treatment of the reference nucleus ^{40}Ca.

In the folding model description of the real optical potential for nuclei other than the reference one (^{40}Ca) the nuclear density ρ_m (eq. (7)) is expressed as a sum of a 2-parameter Fermi form normalized to the correct number of nucleons (A) and an FB series normalized to a volume integral of zero, thus representing a

re-distribution of nucleons relative to the initial Fermi distribution

$$\rho_m(r) = \rho_o(r) + \sum_{n=1}^{N'} \beta_n \, j_o \left(\frac{n\pi r}{R'_c}\right). \qquad (12)$$

Fits to the data are made, using the effective interaction (9) and (11), by varying the nuclear density parameters ρ_o (initially) and β_n (finally) together with the imaginary potential. Variations of the parameters λ and γ are also considered [10,24,32] as one cannot rule out such variations for finite nuclei. It has been found that very small variations of λ and γ of the order of 5 % do indeed improve slightly the fits to the data and the consistency with the phenomenological FB potentials (see Appendix B). Compared to the previous work [5], two additional refinements are included in the present application of the FB folding model. The first is concerned with negative densities which sometimes occur at large radial distances r, a feature also observed in FB-analyses of elastic electron scattering. To suppress such unphysical negative densities we introduced a constraint into the fitting process in the form

$$\chi^2_{total} = \chi^2_{data} \cdot \{[A - \int |\rho_m(\vec{r})| d\vec{r}]^2 + 1\} \qquad (13)$$

which means that an integrated negative density of one unit doubles the total χ^2. This constraint was found to improve the present analyses, but one should, however, note that the tendency of getting negative densities is much less than in other cases (see Appendix C) and also less than in our previous analyses [5] presumably due to the improved interaction model.

The second refinement is in the way the errors of radial moments of ρ_m are calculated. Unlike the case with the moments of the potentials there is no reduction of errors here due to correlations between two integrals because the volume integral of ρ_m is kept precisely equal to A. However, when comparing radial moments of ρ_m and of the corresponding (folded) potential there are correlations (within a given fit) between the two moments with the result that the ratios between moments of ρ_m and of ReU are determined very accurately. Indeed, it has been observed

that these ratios are extremely stable against variations in the numerical procedure (choice of N′ and R_c') contrary to the moments themselves. We could, therefore, combine the ratios obtained from the folding model with the moments of the potential obtained from fits of the potential itself to obtain moments of ρ_m which are generally more accurate than those calculated directly from ρ_m.

With the above methods we obtained nuclear matter densities $\rho_m(r)$ and the corresponding radial moments for all investigated nuclei. The reference nucleus ^{40}Ca was included in the FB-density analysis and treated on equal footings as the other nuclei for two reasons. First, the re-determination of $\rho_m(r)$ with a fixed effective αN-interaction and a flexible FB-density is a kind of self-consistent test of the validity of the folding model approach. Second, the parameters of the effective interaction are only determined within some error bars (see above) resulting from the experimental errors of the ^{40}Ca cross sections. The errors of the interaction parameters are converted into an error band of the density of ^{40}Ca in this re-analysis varying the FB-coefficients of ρ_m. When finally isotopic or isotonic density differences are computed these errors are quadratically added. Hence, the total errors of the differences contain also the uncertainties due to the effective interaction.

III RESULTS

A. Optical Potentials

The phenomenological optical potential analyses using the FB-description of the real potential were performed with numbers of FB-coefficients in the range N=9 - 12 and with cut-off radii in the range R_c=10 - 12 fm. Twelve individual fits were made for each target nucleus the results of which were averaged as described in Ref. 17. The analyses were performed with the optical model codes MODINA[33] and ANALPHA[34]. These

codes are different in the method used to integrate the Schrödinger equation, use different χ^2-minimizing subroutines which compute the error correlation matrix and were each run on computers of different numerical accuracies. Nevertheless, all results agreed within five digits which should be regarded as a convincing test of the numerical procedures. The analyses lead to values of χ^2/F in the range 1.4 to 2.7. The fits to the data are very good as has been demonstrated before for the even A targets [13-15] and as demonstrated in Fig. 1 for the new experimental results for ^{43}Ca.

Table I summarizes the values of the volume integrals (divided by 4A) of the real and imaginary optical potentials, various integral moments $\langle r^k \rangle^{1/k}$ of the real potentials (including the rms radius $\langle r^2 \rangle^{1/2}$) and the rms radii of the imaginary potentials. The errors of the higher radial moments $\langle r^4 \rangle$, $\langle r^6 \rangle$ indicate the accuracy to which the potentials are determined at large radii. Also shown are values of rms radii for the proton distribution [2] whose uncertainties are much smaller than those quoted for the rms radii of the potential. Fig. 2, as example, shows the real optical potentials of the neighboring even and odd A nuclei ^{42,43}Ca and ^{50}Ti, ^{51}V. The error band for ^{51}V is somewhat broader in the nuclear interior as compared to the other nuclei because the experimental data extend only up to $\theta_{CM} = 65°$ (being, however, clearly beyond the nuclear rainbow angle). It should be noted that for both odd A nuclei a depression of the real optical potential in the nuclear interior is indicated which is not observed for any of the even A nuclei.

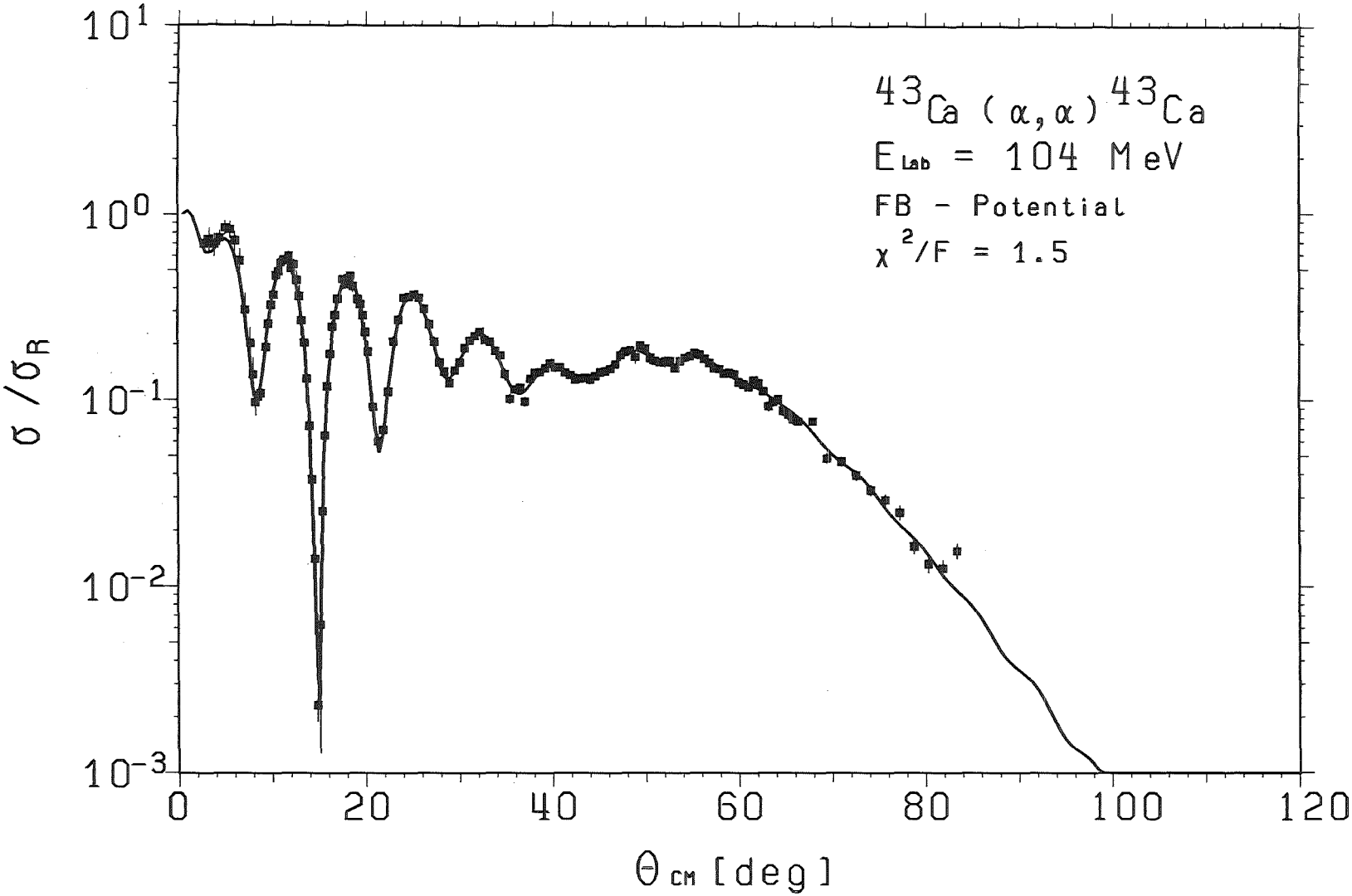

Fig. 1 Differential cross sections divided by the Rutherford cross sections for the elastic α particle scattering by ^{43}Ca. The solid curve is the result of a Fb-potential analysis.

Table I Volume integrals and various radial moments of the real (index v) and imaginary (index w) optical potentials. Also shown are rms radii of the proton distributions $\langle r_p^2 \rangle^{1/2}$. [2]

Target	χ^2/F	$-J_v/4A$ (MeV fm^3)	$\langle r_v^2 \rangle^{1/2}$ (fm)	$\langle r_v^4 \rangle^{1/4}$ (fm)	$\langle r_v^6 \rangle^{1/6}$ (fm)	$-J_w/4A$ (MeV fm^3)	$\langle r_w^2 \rangle^{1/2}$ (fm)	$\langle r_p^2 \rangle^{1/2}$ (fm)
^{40}Ca	2.2	324.8 ± 3.0	4.345 ± 0.022	4.832 ± 0.033	5.276 ± 0.052	103.0	4.934	3.386
^{42}Ca	2.6	316.2 ± 3.0	4.373 ± 0.025	4.851 ± 0.039	5.287 ± 0.060	110.3	4.931	3.422
^{43}Ca	1.5	308.4 ± 5.0	4.344 ± 0.030	4.826 ± 0.043	5.259 ± 0.067	103.0	5.033	3.410
^{44}Ca	2.7	313.8 ± 3.1	4.404 ± 0.025	4.874 ± 0.037	5.300 ± 0.056	111.5	4.959	3.439
^{48}Ca	2.3	324.3 ± 4.9	4.508 ± 0.029	5.023 ± 0.041	5.498 ± 0.059	93.8	5.109	3.409
^{50}Ti	1.6	304.0 ± 3.6	4.446 ± 0.023	4.901 ± 0.031	5.297 ± 0.048	93.2	5.048	3.529
^{51}V	1.4	305.9 ± 8.0	4.515 ± 0.033	4.970 ± 0.050	5.371 ± 0.091	90.1	5.152	3.521
^{52}Cr	1.5	300.4 ± 3.8	4.460 ± 0.024	4.940 ± 0.036	5.367 ± 0.056	96.2	5.088	3.549

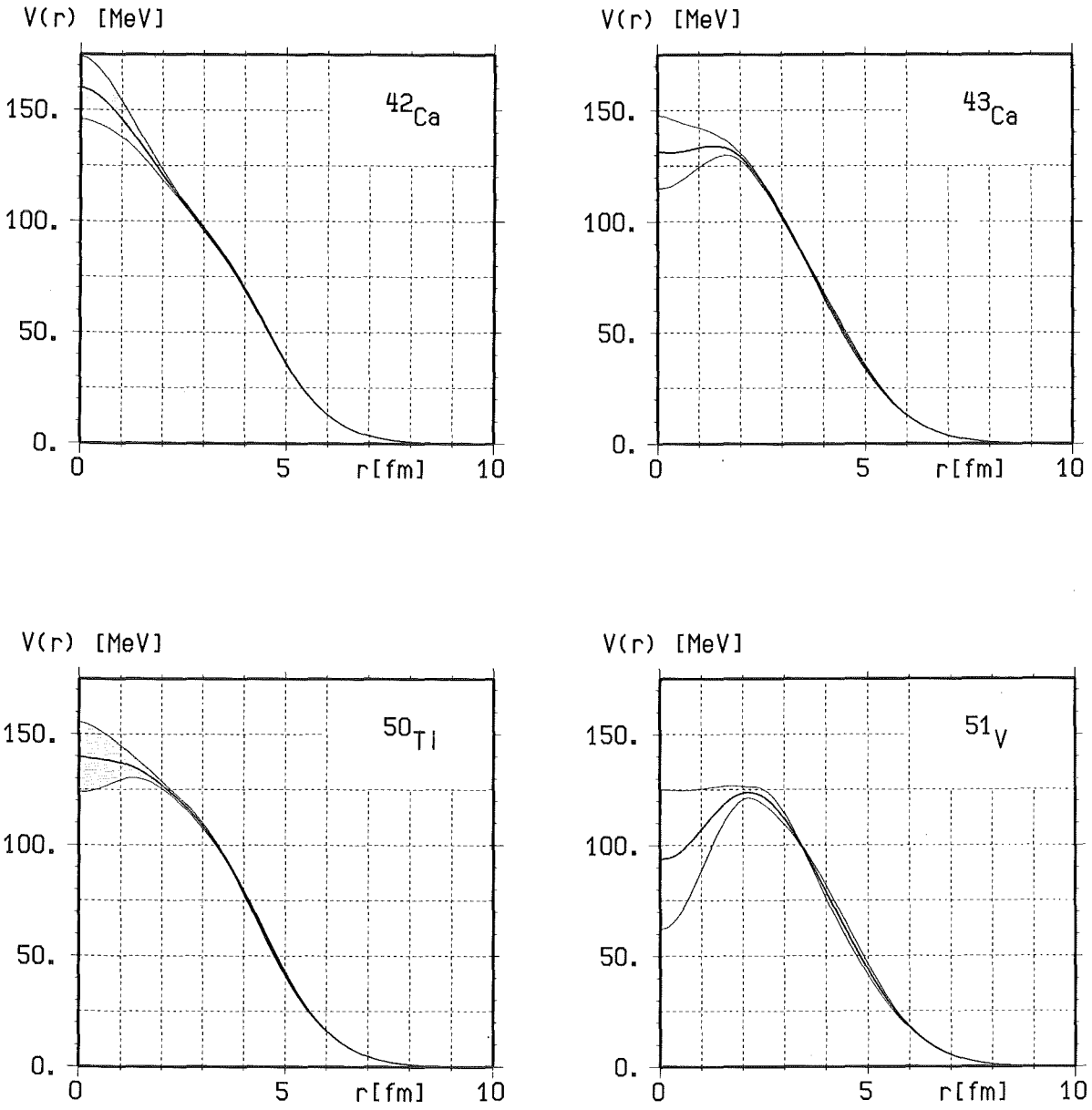

Fig. 2 Real optical α-nucleus potentials for $^{42,43}Ca$, ^{50}Ti, ^{51}V from FB-analyses of elastic α particle scattering. The shaded areas indicate the error band obtained from the FB correlation matrix.

The differences between the real parts of the optical potentials along the isotopic and isotonic chains studied are shown in Fig. 3. The differences in the figure have been multiplied by $4\pi r^2$ to emphasize the regions which significantly contribute to the various radial moments. The potentials have been normalized (before subtraction) to their respective mass number A so that the differences could in principle be compared with differences of nuclear densities which correspond to the radial wave function R(r), where $\Psi \sim R(r)/r$. However, we note that due to the fairly long range of the effective interaction which connects the two distributions, it is not expected that the two distributions will exactly match.

Differences between the potentials for the even isotopes of Calcium clearly show that when an even number of neutrons is added to the ^{40}Ca core, the extra potential is concentrated in the surface region of the potential. This extra potential is centered around r = 4.5 - 5 fm and it has a total spread at half maximum of about 2.8 - 3.2 fm. Considering the fairly small (and non-monotonic) change of the rms radius of the proton distribution (see Table I) along the same isotopic sequence the present results for the optical potentials are strongly suggestive of being associated with the $1f_{7/2}$ neutrons added to the ^{40}Ca core. The values of rms radii $\langle r^2 \rangle^{1/2}$ summarized in Table I are consistent with this picture although the uncertainties in the radii are too large to make the picture conclusive. The differences plotted in Fig. 3 are probably more representative of the isotopic effects than are the values of rms radii.

Differences between the potentials for the even N = 28 isotones ^{48}Ca, ^{50}Ti, ^{52}Cr (Fig. 3, lower row) display a somewhat different character compared to the corresponding differences for the isotopes. The extra potential appears to be less peaked than it is the case for the isotopes with a definite broadening towards smaller radii. One must conclude that the addition of an even number of $1f_{7/2}$ protons to the ^{48}Ca core which increases monotonically the rms radius of the proton distribution (see Table I) is also associated with an inwards shift of neutrons. This picture is supported by the values

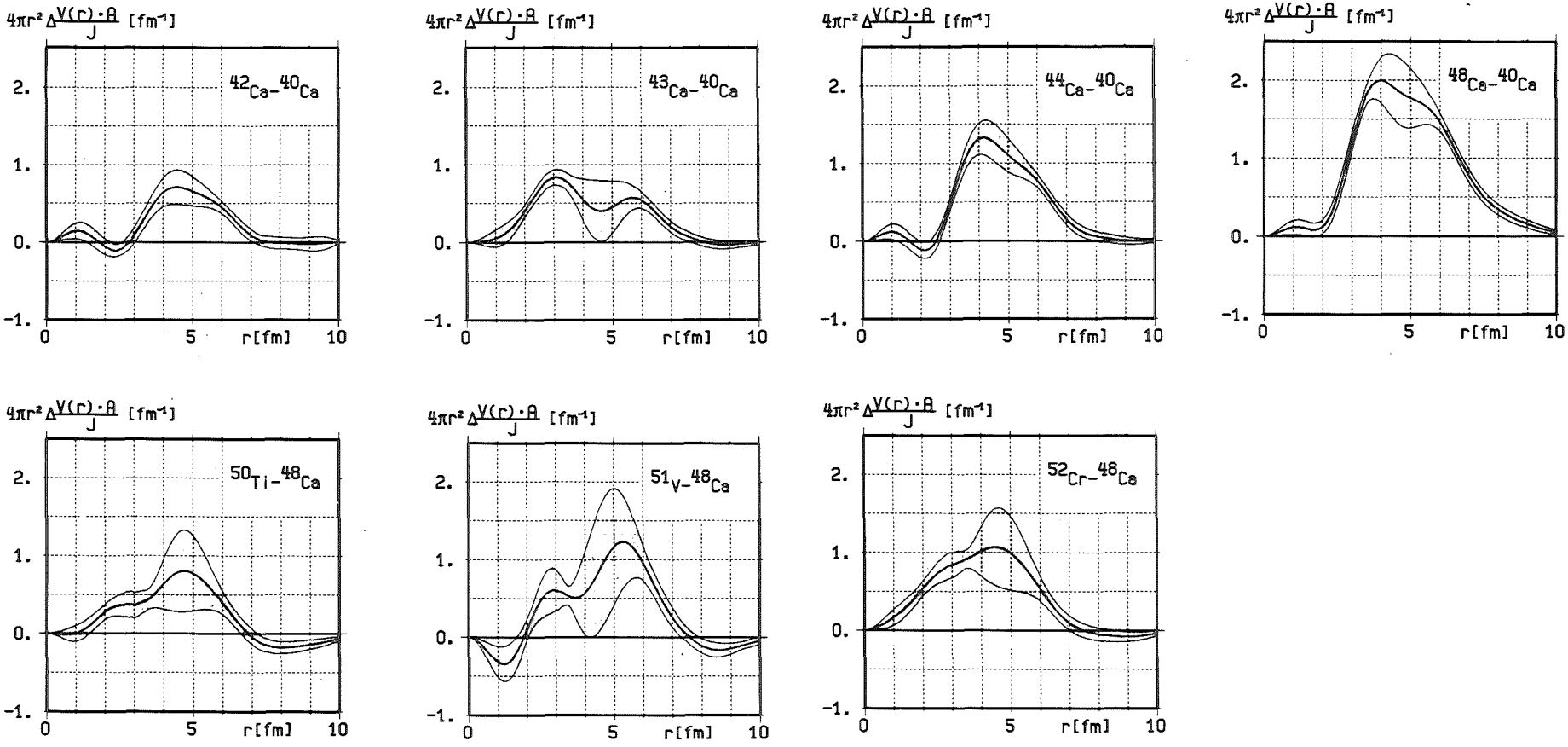

Fig. 3 Differences between the real optical potentials normalized to their respective mass numbers of the Ca isotopes (upper row) and the N = 28 isotones (lower row) multiplied by $4\pi r^2$. The shaded areas indicate the error band obtain from the FB-analyses.

of rms radii in Table I which show that for the isotonic sequence the radius of the potential tends to decrease whilst the proton radius increases significantly.

The odd A nuclei ^{43}Ca and ^{51}V display a very interesting behavior of the extra potentials relative to their respective cores of ^{40}Ca and ^{48}Ca. For ^{43}Ca - ^{40}Ca the extra potential is strongly shifted towards smaller radii, relative to the neighboring isotopes whereas for ^{51}V - ^{48}Ca the extra potential is shifted towards larger radii relative to the neighboring isotones. It is premature to further speculate about the nuclear structure significance of this odd-even effect because the analysis of the data for the odd nuclei was done in the same way as for the even A targets, namely without explicitly including effects due to the non-zero target spin, ground state quadrupole moment ect. However, this odd-even effect and its possible opposite behavior for isotones and isotopes is worth mentioning.

Concluding the results on optical potentials one should keep in mind that the optical potentials on the one hand are the quantities best determined by experiment and marked with only weak and general model assumptions like the optical model itself. On the other hand, the interpretations of the observed potential differences in terms of nuclear structure effects are strongly based on the assumption that the potentials are closely related to the nuclear densities and that details of the reaction mechanism do not change for the studied target nuclei. If the latter is not strictly the case the interpretations may change.

B. Nuclear density distributions

A more direct access to the nuclear density distributions is provided by the folding model approach. We use the folding model with a phenomenological parametrized effective αN-interaction "calibrated" on ^{40}Ca as described in Sect. II B. Hence, the results for ^{40}Ca are most important for the subsequent conclusions and we present them in detail here.

Table II: Quantities of the real and imaginary optical potentials and rms radii of the nuclear matter density of ^{40}Ca from different analyses

Procedure	χ^2/F	$-J_v/4A$ (MeV fm^3)	$\langle r_v^2\rangle^{1/2}$ (fm)	$\langle r_v^4\rangle^{1/4}$ (fm)	$\langle r_v^6\rangle^{1/6}$ (fm)	$-J_w/4A$ (MeV fm^{-3})	$\langle r_w^2\rangle^{1/2}$ (fm)	$\langle r_m^2\rangle^{1/2}$ (fm)
A	2.6	320.0	4.345	4.837	5.287	102.0	4.814	3.369
B	2.8	320.1	4.344	4.835	5.284	102.6	4.901	3.371
C	2.1	320.5	4.350	4.839	5.287	102.3	4.908	3.377 ± 0.017

A: Density from Ref. 27 fixed, effective interaction varied

B: Effective interaction from proc. A fixed, 2-parameter Fermi distribution varied

C: As proc. B, but FB-density varied

In Table II characteristic quantities of the folded optical potentials and of the nuclear matter densities are compiled for the three steps of the analysis. In case A the nuclear density distribution was kept fixed as given by Brown et al. [27] and the parameters of the effective interaction were varied. Case B is the result of the first step of the re-analysis with fixed interaction and a 2-parameter Fermi distribution fitted to the data. We emphasize that this is an important step in the test of self-consistency and radial sensitivity [11] because the resulting Fermi distribution considerably deviates from the distribution used in step A (c.f. Fig. 4). In the final step C only the FB coefficients β_n were varied. The corresponding nuclear density distributions from step A - C are displayed in Fig.4 clearly indicating the consistency of the method. It should be noted that the radial sensitivity of the folding model analysis has been considerably improved as compared to previous claims[11] due to the modified local density approximation. Considering the value n = 0.2 (eq. 11) this is clearly understood since the smearing effect of the density-dependence is much reduced (as compared to n = 1, the previous approach) when going from the nuclear density to the potential by folding. The integral quantities of the folded optical potentials quoted in Table II should be compared to the corresponding numbers given in Table I for the phenomenological FB-potential demonstrating the consistency between both descriptions. We also note that the optical potentials themselves obtained from cases A and C are inside the error band of the FB-potential over the whole radial region. Case B shows small deviations at radii r = 0 - 2 fm and r = 7 - 10 fm as expected from Fig. 4.

Folding model analyses of all studied target nuclei were performed with a modified version of the code MODINA [33] varying 6 - 9 FB-coefficients. The cut-off radii ranged from $R_c' = 6.5$ fm to 7.5 fm. The convergence was as fast as for the FB-potential analyses (in contrast to the previous work [5]). The averaged results are compiled in Tables III and IV.

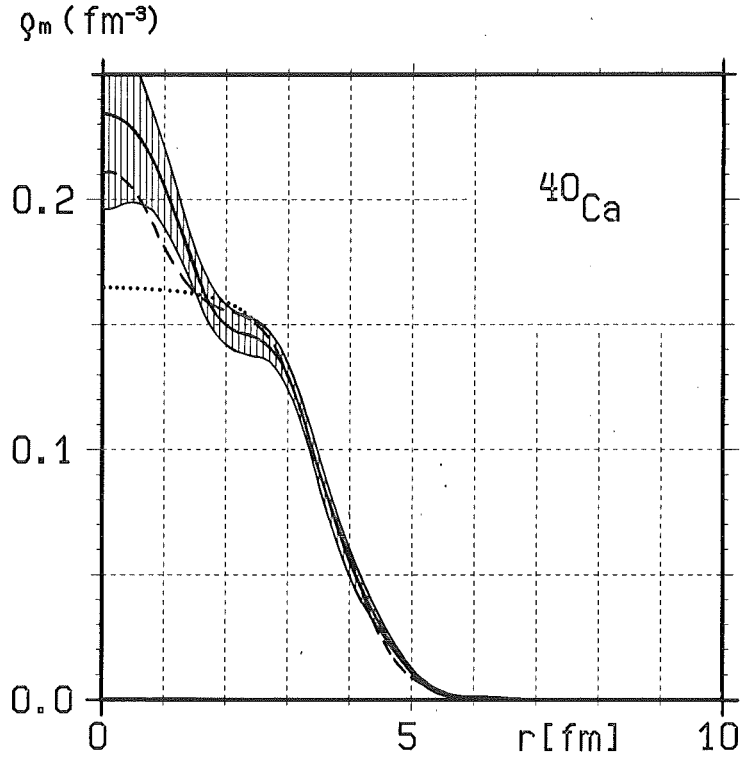

Fig. 4 Nuclear matter density distributions of ^{40}Ca

Dashed line: ρ_m from Ref. 27 (Proc. A)

Dotted line: Fermi-distribution (Proc. B)

Solid line and dashed area: FB-density with error band (Proc. C)

The good consistency between the phenomenological and folding model potentials which is obvious from Tables I and III together with the very good reproduction of the experimental cross sections, as represented by the values of χ^2/F in Table III, is the best support for the present procedure which, from a more fundamental point of view, is oversimplified. Such a consistent picture - to our knowledge - has not been achieved with any other microscopic description of α particle scattering data of the quality provided by the present experiments. The small deviations of the parameters γ and λ from the value requested for the "calibration" nucleus ^{40}Ca do not deteriorate this picture since the changes show obvious tendencies which can be explained by the observed features of the optical potentials (see above) due to the different nuclear structure (see Appendix B).

Table III Moments of the real and imaginary optical potentials obtained in folding model analyses using FB-densities. The last columns show the values of the parameters λ and γ used (eq. 12)

Target	χ^2/F	$J_V/4A$ (MeV fm^2)	$\langle r_V^2\rangle^{1/2}$ (fm)	$\langle r_V^4\rangle^{1/4}$ (fm)	$\langle r_V^6\rangle^{1/6}$ (fm)	$J_W/4A$ (MeV fm^3)	$\langle r_W^2\rangle^{1/2}$ (fm)	λ	γ (fm^2)
^{40}Ca	2.1	320.5	4.350	4.839	5.287	102.3	4.908	1.000	1.645
^{42}Ca	2.8	316.7	4.397	4.870	5.299	110.2	4.931	0.987	1.680
^{43}Ca	2.0	317.2	4.403	4.894	5.339	106.3	4.994	0.975	1.569
^{44}Ca	2.8	312.0	4.416	4.888	5.315	112.4	4.965	0.983	1.670
^{48}Ca	2.3	319.6	4.485	4.988	5.446	95.4	5.099	1.000	1.568
^{50}Ti	1.7	312.0	4.501	4.971	5.395	96.3	5.044	0.968	1.574
^{51}V	2.2	317.2	4.553	5.023	5.442	94.7	5.112	0.971	1.539
^{52}Cr	1.4	302.2	4.480	4.963	5.400	97.3	5.073	0.963	1.573

Table IV Root-mean-square radii for the nuclear density distributions obtained from folding model analyses using FB-densities (column 3) and from implicit folding interpretation of the optical potential results of Table I (column 4). In the last two columns rms radii of the proton distributions [2] and of the neutrons distributions as determined from columns 3 and 5 are compiled.

Target	folding model fits χ^2/F	$\langle r_m^2 \rangle^{1/2}$ (fm)	implicit folding interpretation $\langle r_m^2 \rangle^{1/2}$ (fm)	protons $\langle r_p^2 \rangle^{1/2}$ (fm)	neutrons $\langle r_n^2 \rangle^{1/2}$ (fm)
^{40}Ca	2.1	(3.38 ± 0.02)	3.37 (fixed)	3.386	(3.37 ± 0.04)
^{42}Ca	2.8	3.43 ± 0.02	3.41	3.422	3.45 ± 0.04
^{43}Ca	2.0	3.48 ± 0.03	3.37	3.410	3.54 ± 0.06
^{44}Ca	2.8	3.45 ± 0.02	3.45	3.439	3.46 ± 0.04
^{48}Ca	2.3	3.51 ± 0.03	3.58	3.409	3.58 ± 0.05
^{50}Ti	1.7	3.55 ± 0.02	3.50	3.529	3.56 ± 0.04
^{51}V	2.2	3.63 ± 0.03	3.59	3.521	3.72 ± 0.07
^{52}Cr	1.4	3.54 ± 0.02	3.52	3.549	3.54 ± 0.04

The rms nuclear matter radii obtained from the implicit folding interpretation of the optical potentials (Table IV, column 4) agree satisfactorily (with the exceptions of ^{43,48}Ca) with those obtained from the explicit FB folding model. The implicit folding interpretation is based on the assumption of additivity of mean square radii which is strictly valid only for a density-independent interaction.[13] This agreement is due to the fact that the density dependence mainly influences the volume integral of the folded optical potential rather than the rms radius [13,35], an observation which is even more pronounced for the "mixed" LDA [12] used in the present folding model analyses.

For comparison, in Table IV (column 6) the rms radii of the neutron distributions $\langle r_n^2 \rangle^{1/2}$ are also compiled as determined from columns 3 and 5 via the relation

$$\langle r_n^2 \rangle = \frac{1}{N} \cdot (A \langle r_m^2 \rangle - Z \langle r_p^2 \rangle). \qquad (14)$$

In contrast to the radii of the proton distributions (Table IV, column 5) the extracted rms matter radii of the even Ca-isotope chain increase monotonically with mass number whereas the matter radii of the even isotones remain nearly constant. A considerable difference between proton and total matter distribution radii occurs only for ^{48}Ca indicating a neutron skin for this nucleus. The matter radii quoted for the odd nuclei ^{43}Ca, ^{51}V should be regarded as preliminary because the target spin and quadrupole moments have been ignored in the analysis which may change the results. Keeping this in mind, the particular behavior of the odd mass nuclei is, nevertheless, worth mentioning, featuring an odd-even staggering effect with the odd nucleus having a larger radius than its even neighbors. This behavior is opposite to the well known odd-even staggering of charge radii in isotope chains where the odd nuclei have smaller radii than their even neighbors.

Examples of extracted nuclear matter densities are displayed in Fig. 5 clearly showing structures also in the surface region which makes obvious the need to use FB-densities instead of the widely used Fermi form.

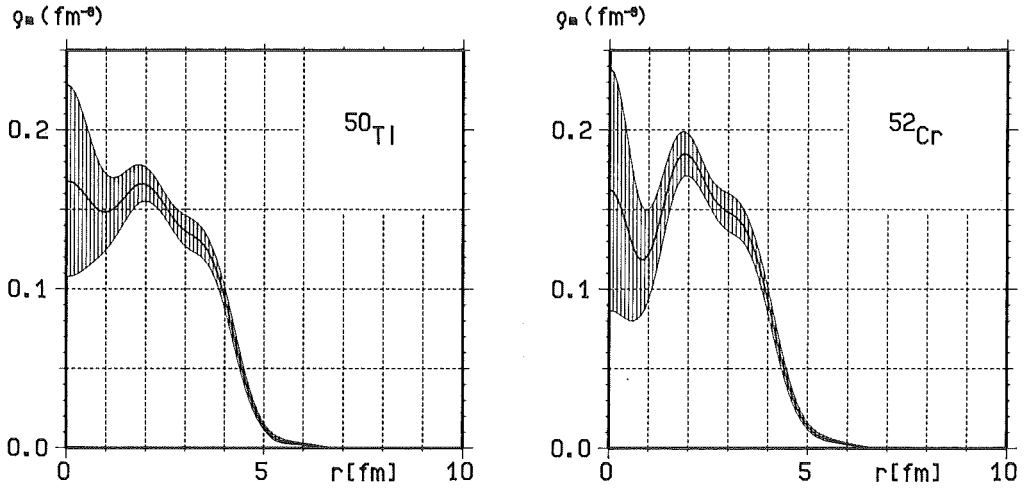

Fig. 5 Nuclear matter densities of ^{50}Ti and ^{52}Cr obtained from folding model analyses. The shaded areas indicate the error bands.

Differences between the nuclear matter distribution of the Ca isotope chain (upper row) and the N=28 isotone chain are shown in Fig. 6. As for the optical potentials (fig.3) the differences are multiplied by $4\pi r^2$. Although the error bands of the density differences are larger than for the potentials, pronounced structures occur which are consistent with those of the potential differences. Due to the obvious smearing effect of the folding integral, however, the structures of the density differences are sharper. One observes similar shapes of the differences of the even Ca-isotopes characterized by three maxima at r≈2.4, 3.8, 5.5 fm and a negative region around r = 1.3 fm. The dominant maximum

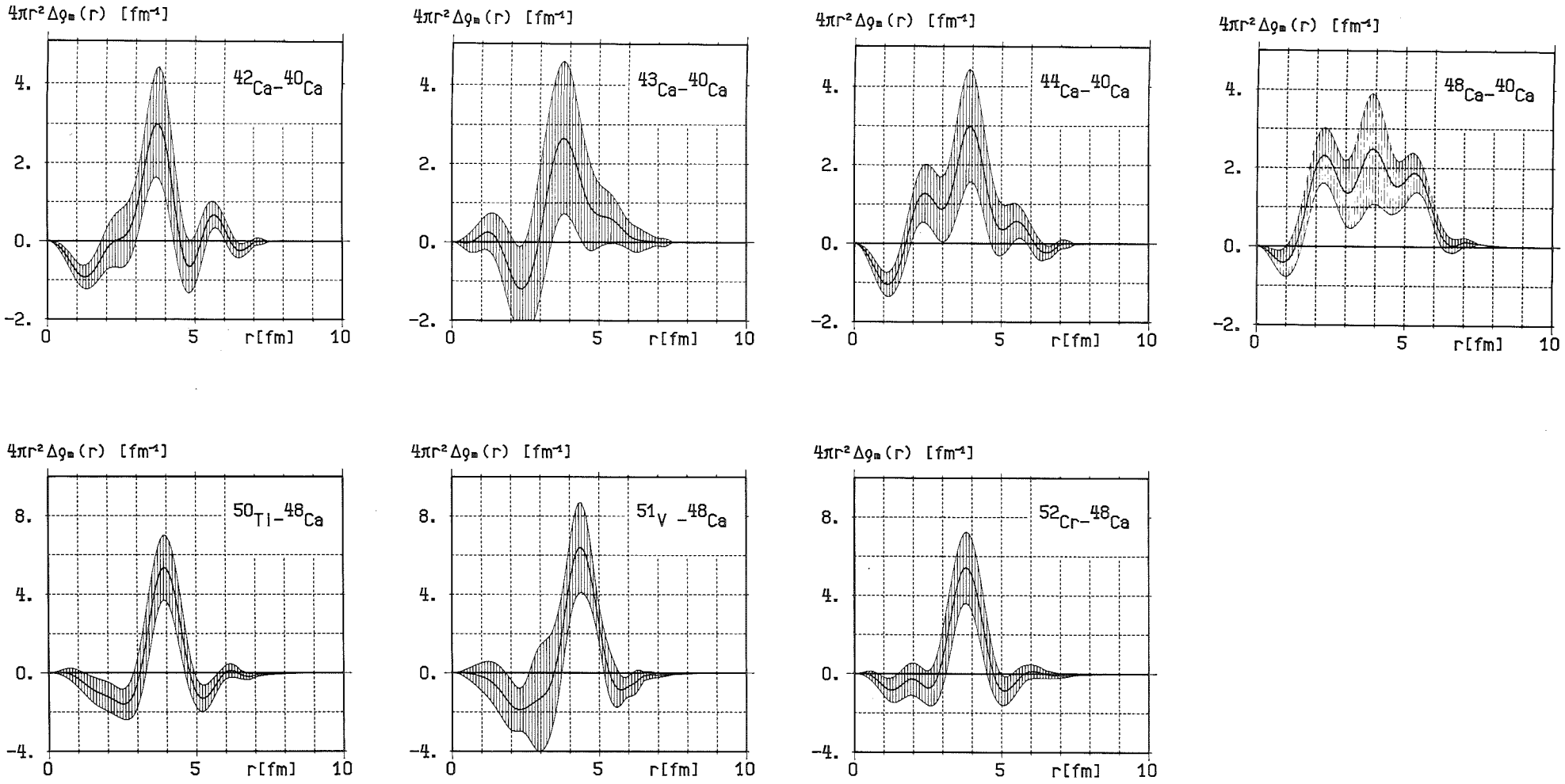

Fig. 6 Differences of nuclear matter densities and their corresponding error bands (shaded area) of the Ca isotope chain (upper row) and the N = 28 isotone chain (lower row). Note the different scales.

at r ≈ 3.8 fm coincides with the radial position of $1f_{7/2}$ nucleons as determined from magnetic electron scattering [36] and from nucleon transfer reactions.[37] The positions of the satellite peaks at r ≈ 2.4 and 5.5 fm can be associated with s-d-shell and f-p-shell nucleons.

The nuclear matter density differences of the even N = 28 isotones are also characterized by a pronounced maximum peaking at r ≈ 3.9 fm whereas negative regions are indicated around r ≈ 2.5 fm and r = 5.5 fm. These negative regions should be interpreted in connection with the matter density of ^{48}Ca where one observes nuclear matter concentrated around r = 2.5 and 5.5 fm which seems to move into the r = 3.9 fm shell when adding protons leading to the nuclei ^{50}Ti, ^{52}Cr. When comparing the differences between nuclear densities (fig. 6) with the differences between the optical potentials (fig. 3) it becomes clear that although they are qualitatively consistent with each other there is no simple connection between the two types of quantities. In addition to the smearing-out effect of eq. (7) the situation is further complicated in the present case due to the density dependence of the effective interaction which means that fig. 3 is not connected to fig. 6 by a simple folding relation. The small renormalizations of the potentials according to their different specific volume integral (c.f. Sec. III.A) which form the basis to fig. 3 complicate even further the relation between the two types of differences. Caution is therefore required when inferring isotopic and isotonic effects in nuclear densities from differences of optical potentials.

The odd mass number nuclei ^{43}Ca, ^{51}V in general match into the corresponding chains of differences of even mass number nuclei but show different behavior when compared with each other. Whereas the difference between ^{43}Ca and ^{40}Ca is rather smooth we observe for ^{51}V a large peak of added nucleons in a region around r = 4.5 fm as compared to ^{48}Ca.

In order further to enlight the apparently different behavior of the isotope and isotone chains the nuclear matter densities of the N = 28 isotones are compared to ^{40}Ca as shown in fig. 7. These differences smoothly continue the behavior of the Ca-isotope differences featuring a main maximum at the radial position of the 1 $f_{7/2}$ shell which is continuously increasing when adding protons. Additionally, two smaller maxima are observed (to be associated with the s-d- and f-p-shells) which are largest for ^{48}Ca.

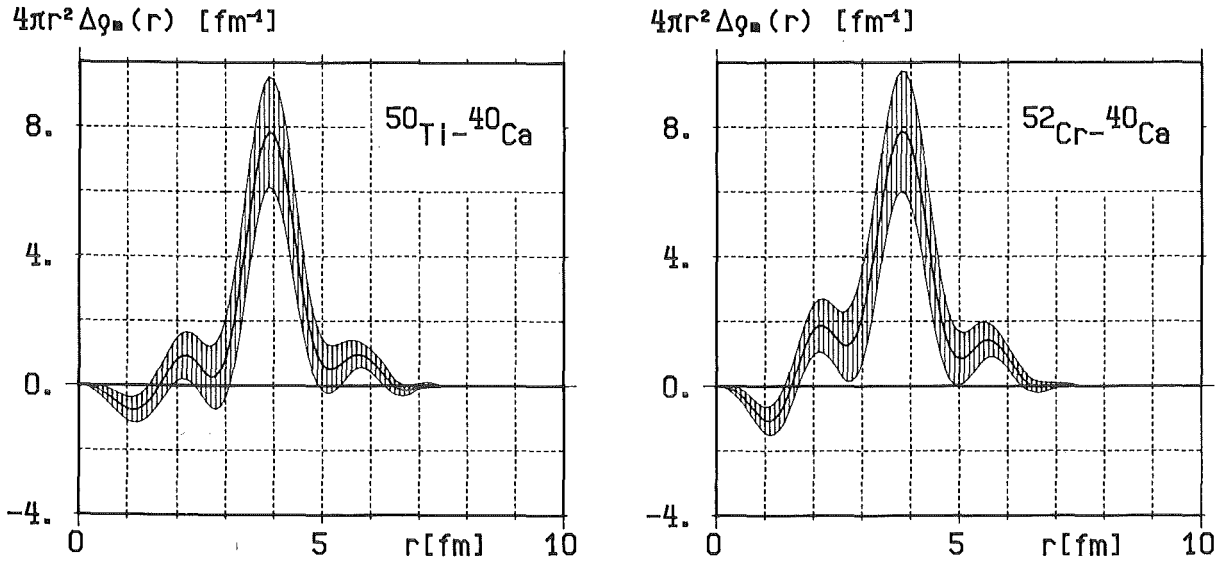

Fig. 7 Differences of nuclear matter densities of even N = 28 isotones as compared to ^{40}Ca, with the corresponding error bands (shaded areas)

IV DISCUSSION

The elastic scattering of 104 MeV α particles by $1f_{7/2}$ shell nuclei has been shown to be a sensitive tool for determining differences of the real optical potentials when using flexible parametrization like the FB-method. Within a reasonable reaction model - the single folding model - these differences can directly be interpreted in terms of differences of the nuclear matter distributions. Although the single folding model is a rather simple microscopic description of the optical potential and treats important effects like density-dependence of the effective projectile-nucleon interaction in a phenomenological way the folded optical potentials reproduce the "model independent" FB-potentials exceptionally well and fit the experimental data as well as the latter. Hence, one may be confident that differences between properties of neighboring nuclei are reliably determined by this model.

The results on the even Ca-isotopes are in full agreement with those previously determined from the same data. [5] Some details, however, are obtained in a more conclusive form due to the improved procedures and - as a consequence of this - due to reduced errors. There is also very good agreement with the results of other experimental methods for the isotope chain [6,8,9] although the different methods are sensitive to slightly different quantities [11]. Corresponding results for the isotone chain are not available in the literature . The present experiments are mainly sensitive in the range between r = 2 - 6 fm [1,11] (see also Appendix D) covering the whole nuclear surface from the outermost tail up to the central region of maximum density. In this region the densities are determined with a rather constant relative error of about 5 % and no systematic errors due to the particular choices in the FB-analyses were observed. Outside this radial region the relative error increase considerably and uncertainties due to the choice of R_c' and N'(see eq. 12) are not negligible in particular in the nuclear interior. These uncertainties due to the model can not fully be included into the displayed error bands since there is no well

founded procedure available to do this. One should keep this in mind when regarding the differences of the radial shapes of the nuclear matter densities. The integral quantities of the nuclear densities like the rms radius and higher moments and their respective errors, however, are negligibly influenced by the choices in the FB-folding analyses.

The rms radii of the matter and neutron distributions are - within the error bars - in full agreement with previous experimental results [1,5,6,8,9] and theoretical calculations [1,27,29-31,38] confirming the growing consensus obtained by the various methods when less model dependent procedures are applied.

As one of the most important results concerning the radial shapes of the nuclear matter densities one should emphasize the finding that adding neutrons and protons to the $1f_{7/2}$ shell does not only cause changes of the total nucleon density distribution in a well-defined radial region associated with the $1f_{7/2}$ shell but also cause considerable changes in a wide radial range with some structures possibly due to neighboring shells. Similar effects have also been observed for the differences of the nuclear *charge* distributions [1,7,39,40]. (For the Ca-isotope chain this is a trivial effect since changes of the charge distributions in the $1f_{7/2}$ region inevitably cause changes in other radial regions due to the constant total charge of the isotopes). In the isotone sequence ^{48}Ca, ^{50}Ti, ^{52}Cr the added charge is not only concentrated around $r \approx 4.0$ fm as expected but important contributions are also observed at $r \approx 2.2$ fm with a minimum of the difference at $r \approx 3.0$ fm.[39,40] These results from completely different experiments confirm the observed structures of the density differences from the present investigations which systematically show minima around $r \approx 3$ fm and $r \approx 5$ fm indicating "forbidden" radial regions when adding nucleons to the Ca-core. In shell model calculations [27,41] similar structures in the matter density differences are indicated in particular for ^{48}Ca but are much less pronounced. In general, the theoretical density differences [27,29-31,38,42] show a smooth bell shape with a rather constant width of 3.5 fm (FWHM) for all cases displayed in this

paper including also the odd nuclei. This global behavior which is in contrast to the present findings may indicate that even advanced microscopic theories may neglect important effects or may be too strongly adjusted on particular experimental results (mainly of electromagnetic probes) so that effects due to the neutrons are not sufficiently considered. One should not forget, however, that ^{48}Ca is an exceptional nucleus due to its very large neutron excess and, therefore, differences between nuclear densities might reflect this point.

The odd mass number nuclei ^{43}Ca, ^{51}V treated in this report on equal footings with the even ones show important deviations from the latter and from each other. The results presented here (in particular those for the densities) have to be regarded as preliminary due to target spin and quadrupole moments so far ignored. Nevertheless, the present results encourage further investigations on odd-even effects of neutron and matter distributions.

The authors would like to thank Prof. Dr. G. Schatz for his encouraging interest in our work and Prof. Dr. P.E. Hodgson and Dr. B.A. Brown for fruitful discussions and suggestions. We thank Dr. H.J. Emrich for providing us with several experimental and theoretical results prior to publication. The help of Dr. J. Buschmann and Miss D. Dürrschnabel with the numerical calculations and preparations of figures is greatfully acknowledged.

References

1 Proceedings of the International Discussion Meeting, Karlsruhe, 1979, edited by H. Rebel, H.J. Gils, and G. Schatz, Kernforschungszentrum Karlsruhe, Report KfK 2830, (1979)

2 H.D. Wohlfahrt, E.B. Shera, M. V. Hoehn, Y. Yamazaki, G. Fricke, and R.M. Steffen, Phys. Lett. 73B, 131 (1978); H.D. Wohlfahrt, E.B. Shera, M.V. Hoehn, Y. Yamazaki, and R.M. Steffen, Phys. Rev. C 23, 533 (1981)

3 F. Träger, Z. Phys. A 299, 33 (1981)

4 A. Andl, K. Bekk, S. Göring, A. Hanser, G. Nowicki, H. Rebel, G. Schatz, and R.C. Thompson, Phys. Rev. C 26, 2194 (1982)

5 E. Friedman, H.J. Gils, H. Rebel, and Z. Majka, Phys. Rev. Lett. 41, 1220 (1978); H. J. Gils, E. Friedman, Z. Majka, and H. Rebel, Phys. Rev. C 21, 1245 (1980)

6 G. Igo, G.S. Adams, T.S. Bauer, G. Pauletta, C.A. Whitten Jr., A. Wreikat, G.W. Hoffmann, G.S. Blanpied, W.R. Coker, C. Harvey, R.P. Liljestrand, L. Ray, J. Spencer, H.A. Thiessen, C. Glashausser, N.M. Hintz, M.A. Oothoudt, H. Nann, K.K. Seth, B.E. Wood, D.K. McDaniels, and M. Gazzaly, Phys. Lett. 81 B, 151 (1979); L. Ray, Phys. Rev.C 19, 1855 (1979); L. Ray, G.W. Hoffmann, M. Barlett, J. McGill, J. Amann, G. Adams, G. Pauletta, M. Gazzaly, and G.S. Blanpied, *ibid.* 23, 828 (1981)

7 H.J. Emrich, G. Fricke, G. Mallot, H. Miska, H.-G. Sieberling, J.M. Cavedon, B. Frois, and D. Goutte, International Conference on Nuclear Structure, Amsterdam, 1982, Nucl. Phys. A 396, 401c (1983)

8 G. Pauletta, G. Adams, M.M. Gazzaly, G.J. Igo, A.T.M. Wang, A. Rahbar, A. Wreikat, L. Ray, G.W. Hoffmann, M. Barlett, and J. Amann, Phys. Lett. 106 B, 470 (1981)

9 L. Ray and G.W. Hoffmann, Phys. Rev. C27 2143 (1983)

10 Z. Majka, H.J. Gils, and H. Rebel, Z. Phys. A 288, 139 (1978)

11 E. Friedman, H.J. Gils, and H. Rebel, Phys. Rev. C 24, 1551 (1982)

12 H. J. Gils, Z. Phys. A (submitted)
H. J. Gils, Report KfK 3555, Kernforschungszentrum Karlsruhe (1983)

13 E. Friedman, H.J. Gils, H. Rebel, and R. Pesl, Nucl. Phys. A363, 137 (1981)

14 R. Pesl, H.J. Gils, H. Rebel, E. Friedman, J. Buschmann, H. Klewe-Nebenius, and S. Zagromski, Z. Phys. A 313, 111 (1983)
Report KfK 3378, Kernforschungszentrum Karlsruhe (1983)

15 H.J. Gils, E. Friedman, H. Rebel, J. Buschmann, S.Zagromski, H. Klewe-Nebenius, B. Neumann, R. Pesl, and G. Bechtold, Phys. Rev. C 21, 1239 (1980)

16 E. Friedman and C.J. Batty, Phys. Rev. C 17, 34 (1978)

17 H.J. Gils, E. Friedman, H. Rebel, J. Buschmann, S. Zagromski, H. Klewe-Nebenius, B. Neumann, R. Pesl, and G. Bechtold, Report KfK 2838, Kernforschungszentrum Karlsruhe (1979)

18 A.M. Bernstein, in *Advances in Nuclear Physics*, edited by M. Baranger and E. Vogt (Plenum, New York, 1969)

19 D.F. Jackson and V.K. Kembhavi, Phys. Rev. 178, 1626 (1969)

20 F. Petrovich, D. Stanley, and J. J. Bevelacqua, Phys. Lett. 71 B, 259 (1977)

21 J.-P. Jeukenne, A. Lejeune, and C. Mahaux, Phys. Rev. C 16, 80, (1977)

22 W. D. Myers, Nucl. Phys. A 204, 465 (1973)

23 Z. Majka, Phys. Lett. 76 B, 161 (1978)

24 A.M. Kobos, B.A. Brown, P.E. Hodgson, G.R. Satchler, and A. Budzanowski, Nucl. Phys. A 384, 65 (1982)

25 D.K. Srivastava, Phys. Lett. 113B, 353 (1982)

26 J.-P. Jeukenne and C. Mahaux, Z. Phys. A 302, 233 (1981)

27 B.A. Brown, S.E. Massen, and P.E. Hodgson, J. Phys. G 5, 1455 (1979)

28 I. Sick, J.B. Bellicard, J.M. Cavedon, B. Frois, M. Huet, P. Leconte, P.X. Ho, and S. Platchkov, Phys. Lett. 88B, 245 (1979)

29 J.W. Negele, Phys. Rev. C 1,1260 (1970); J.W. Negele and D. Vautherin, Phys. Rev. C 5, 1472 (1970)

30 X. Campi and D. Sprung, Nucl. Phys. A194, 401 (1972)

31 J. Dechargé and D.Gogny, Phys. Rev. C 21, 1568 (1980)

32 G.R. Satchler and W.G. Love, Phys. Rev. 55, 183 (1979)

33 H.J. Gils, Report KfK 3063, Kernforschungszentrum Karlsruhe (1980)

34 E. Friedman, unpublished program description

35 Z. Majka, H. J. Gils, and H. Rebel, Acta Phys. Pol. B 11, 227 (1980)

36 S.K. Platchkov, J.B. Bellicard, J.M. Cavedon, B. Frois, D. Goutte, M. Huet, P. Leconte, Phan Xuan-Ho, P.K.A. de Witt Huberts, L. Lapikás, and I.Sick, Phys. Rev. C 25, 2318 (1982)

37 J. L. Durell, C. A. Harter, J.N. Mo, and W.R. Phillips, Nucl. Phys. A 334, 144 (1980)

[38] D. Berdichevsky and U. Mosel, preprint (1982)

[39] H. J. Emrich and G. Fricke, private communication of results from H.D. Wohlfahrt

[40] J.W. Lightbody, Jr., J.B. Bellicard, J.M. Cavedon, B. Frois, D. Goutte, M. Huet, Ph. Leconte, A. Nakada, Phan Xuan-Ho, S.K. Platchkov, S. Turck-Chieze, C.W. de Jager, J.J. Lapikás, and P.K.A. de Witt Huberts, Phys. Rev. C. 27, 113 (1983)

[41] B.A. Brown and P.E. Hodgson, private communication

[42] J. Friedrich, P.-G. Reinhard, and N. Voegler, preprint (1982); H. J. Emrich, private communication

Appendix A

Some details of the numerical procedures

The results on optical potentials and nuclear matter densities may - within the quoted errors - slightly depend on particular choices in the numerical procedures like integration step size and matching radius. Therefore, the important values commonly used for all nuclei are given in Table A1. These values are valid only for the optical model code MODINA.[33]

Table A1: Parameter values for the numerical procedures commonly used for all nuclei:

Maximum L-value of partial waves	LMAX = 60
Radial integration step size for Schrödinger equation during the fits	Δr_s = 0.2 fm +)
Radial integration step size for potentials and densities, finally	$\Delta r_{v,\rho}$ = 0.1 fm
Matching radius	R_ψ = 15 fm
Cut-off radius for densities	R_ρ = 10 fm
Cut -off radius for $V_{\alpha N}$	R_v = 31 fm

The Coulomb potentials have been calculated from realistic charge distribution as described in Ref. 33 with Gaussian shape for the α particle and Fermi shape for the target nuclei. The parameter values are compiled in Table A2.

The parameter values used for the "first guess" real optical potentials $V_o(r)$ (eq. (1)) (squared Saxon-Woods form) are given in Table A3. Also compiled are the corresponding best-fit parameters of the imaginary potentials (Saxon-Woods form) and values of χ^2/F.

+) Please note, that the code MODINA [33] uses special numerical procedures which allow rather large step sizes.

Table A2 Parameter of nuclear charge distribution used for computing realistic Coulomb potentials

α particle	Gaussian shape		a_G^{ch} = 1.3227 fm
Target	$c_{ch} \cdot A^{1/3}$ (fm)	a_{ch} (fm)	w_{ch}
^{40}Ca	3.766	0.586	-0.161
^{42}Ca	3.728	0.591	-0.116
^{43}Ca	3.6621	0.55	0.
^{44}Ca	3.748	0.572	-0.095
^{48}Ca	3.7369	0.5245	-0.03
^{50}Ti	3.8413	0.5399	-0.0381
^{51}V	3.91	0.532	0.
^{52}Cr	3.8962	0.55	0.

Table A3 Parameter values of $V_o(r)$ (eq.1) and corresponding best-fit parameters of the imaginary optical potentials (Real potential: squared Saxon-Woods form; imaginary potential: Saxon-Woods form)

Target	χ^2/F	V_0 (MeV)	r_v (fm)	a_v (fm)	$-J_v/4A$ (MeV fm^3)	$\langle r^2_v \rangle^{1/2}$ (fm)	W_0 (MeV)	r_w (fm)	a_w (fm)	$-J_w/4A$ (MeV fm^3)	$\langle r^2_w \rangle^{1/2}$ (fm)
^{40}Ca	3.3	151.9	1.407	1.248	318.0	4.314	20.3	1.607	0.672	101.0	4.935
^{42}Ca	4.1	139.8	1.441	1.203	312.9	4.370	22.0	1.608	0.647	108.6	4.951
^{43}Ca	2.3	155.0	1.392	1.267	314.4	4.375	22.4	1.564	0.710	104.5	4.996
^{44}Ca	3.6	139.4	1.438	1.189	310.0	4.394	24.0	1.578	0.665	112.6	4.973
^{48}Ca	3.3	162.1	1.378	1.274	318.4	4.458	18.9	1.633	0.603	95.0	5.114
^{50}Ti	1.8	147.1	1.408	1.197	307.0	4.469	20.1	1.600	0.582	94.5	5.052
^{51}V	2.3	144.3	1.430	1.195	315.5	4.535	20.0	1.590	0.619	93.4	5.114
^{52}Cr	1.7	157.2	1.367	1.229	300.4	4.456	22.4	1.540	0.667	97.0	5.096

Appendix B

Variations of the density-dependence of different target nuclei

The different nuclear structure of the target nuclei causes small changes in the density-dependence of the effective αN-interaction[12] (see also Sec. III.B). These changes may be accounted for by varying the values of the parameters γ or λ (eq. (10)) individually or together. The dependence of the folding model results on these different choices has been studied using 2-parameter Fermi distributions (F2) for ρ_m the parameter values c_m, a_m of which were varied together with γ or λ and the parameters of the imaginary optical potentials. Fits allowing to vary γ and λ together did not converge in most cases. In addition two examples were studied where λ was kept fixed but different to $\lambda = 1$ and γ was varied. In the first of these examples λ was adjusted to the ratio $\lambda_1(A) = J_v(A)/J_v(^{40}Ca)$ as calculated from Table I, in the second case the average between $\lambda = 1$ and $\lambda_1(A)$ was chosen. The results are compiled in Tables B1 to B5. The results B5 have been used as basis for the final FB density analyses (Sec. III.B).

Table B1

Results with parameters γ and λ fixed as obtained from ^{40}Ca

Target	χ^2/F	γ (fm^2)	λ	c_m (fm)	a_m (fm)	$\langle r^2_m \rangle^{1/2}$ (fm)	$-J_v/4A$ (MeV fm^3)	$\langle r^2_v \rangle^{1/2}$ (fm)	$-J_w/4A$ (MeV fm^3)	$\langle r^2_w \rangle^{1/2}$ (fm)
^{40}Ca	2.80	1.645	1.000	1.0709	0.4900	3.371	320.1	4.344	102.6	4.901
^{42}Ca	5.59	1.645	1.000	1.1401	0.4353	3.470	322.7	4.406	110.4	4.958
^{43}Ca	2.57	1.645	1.000	1.0670	0.4999	3.440	318.4	4.407	106.4	4.973
^{44}Ca	5.36	1.645	1.000	1.1258	0.4387	3.484	319.9	4.426	113.8	4.971
^{48}Ca	5.84	1.645	1.000	1.0722	0.4713	3.490	313.0	4.457	97.4	5.062
^{50}Ti	2.33	1.645	1.000	1.1233	0.4182	3.563	314.5	4.502	96.7	5.051
^{51}V	2.40	1.645	1.000	1.1706	0.3810	3.649	318.0	4.557	95.4	5.096
^{52}Cr	2.32	1.645	1.000	1.0510	0.4777	3.519	308.1	4.498	98.8	5.087

Table B2

Results with the parameter γ fixed and parameter λ optimized

Target	χ^2/F	γ (fm^2)	λ	c_m (fm)	a_m (fm)	$\langle r^2_m \rangle^{1/2}$ (fm)	$-J_v/4A$ (MeV fm^3)	$\langle r^2_v \rangle^{1/2}$ (fm)	$-J_w/4A$ (MeV fm^3)	$\langle r^2_w \rangle^{1/2}$ (fm)
^{40}Ca	2.80	1.645	1.0000	1.0709	0.4900	3.371	320.1	4.344	102.6	4.901
^{42}Ca	3.35	1.645	0.9774	1.1589	0.4071	3.468	315.6	4.399	110.4	4.946
^{43}Ca	2.69	1.645	0.9962	1.0737	0.4902	3.436	317.1	4.402	107.3	4.958
^{44}Ca	3.28	1.645	0.9753	1.1430	0.4117	3.480	312.1	4.418	112.8	4.967
^{48}Ca	3.11	1.645	1.0246	1.0310	0.5368	3.522	321.5	4.496	96.9	5.098
^{50}Ti	1.87	1.645	0.9883	1.1322	0.4018	3.559	310.8	4.496	96.7	5.041
^{51}V	2.41	1.645	1.0027	1.1706	0.3862	3.656	319.2	4.563	95.6	5.101
^{52}Cr	1.60	1.645	0.9864	1.0548	0.4669	3.509	303.4	4.488	98.7	5.072

Table B3

Results with the parameter $\lambda = 1$ fixed and parameter γ optimized.

Target	χ^2/F	γ (fm^2)	λ	c_m (fm)	a_m (fm)	$\langle r^2_m \rangle^{1/2}$ (fm)	$-J_v/4A$ (MeV fm^3)	$\langle r^2_v \rangle^{1/2}$ (fm)	$-J_w/4A$ (MeV fm^3)	$\langle r^2_w \rangle^{1/2}$ (fm)
^{40}Ca	2.80	1.6450	1.000	1.0709	0.4900	3.371	320.1	4.344	102.6	4.901
^{42}Ca	3.15	1.7209	1.000	1.1331	0.4262	3.438	315.8	4.398	109.9	4.938
^{43}Ca	2.56	1.6525	1.000	1.0752	0.4896	3.439	317.9	4.405	106.7	4.969
^{44}Ca	3.19	1.7264	1.000	1.1145	0.4355	3.451	312.4	4.420	112.6	4.962
^{48}Ca	3.26	1.5683	1.000	1.0537	0.5186	3.537	320.6	4.484	96.2	5.104
^{50}Ti	1.92	1.6804	1.000	1.1062	0.4313	3.541	310.6	4.498	96.1	5.043
^{51}V	2.75	1.6464	1.000	1.1578	0.3993	3.642	317.4	4.556	95.6	5.090
^{52}Cr	1.66	1.6826	1.000	1.0223	0.4973	3.486	302.8	4.491	97.8	5.075

Table B4

Results with the parameter $\lambda_1 = J(A)/J(^{40}Ca)$ (J(A) from table 1) fixed, parameter γ optimized

Target	χ^2/F	γ (fm^2)	λ	c_m (fm)	a_m (fm)	$\langle r^2_m \rangle^{1/2}$ (fm)	$-J_v/4A$ (MeV fm^3)	$\langle r^2_v \rangle^{1/2}$ (fm)	$-J_w/4A$ (MeV fm^3)	$\langle r^2_w \rangle^{1/2}$ (fm)
^{40}Ca	2.80	1.645	1.000	1.0709	0.4900	3.371	320.1	4.344	102.6	4.901
^{42}Ca	5.12	1.599	0.974	1.2440	0.3070	3.484	315.0	4.401	110.1	4.938
^{43}Ca	2.46	1.504	0.950	1.0960	0.4780	3.463	318.9	4.391	105.7	4.976
^{44}Ca	3.34	1.614	0.966	1.2210	0.3010	3.485	311.6	4.415	112.6	4.968
^{48}Ca	3.36	1.559	0.999	1.0660	0.5590	3.551	321.4	4.490	97.1	5.087
^{50}Ti	1.87	1.494	0.936	1.1600	0.3750	3.593	312.0	4.487	96.4	5.043
^{51}V	2.32	1.454	0.942	1.1950	0.3650	3.690	319.9	4.550	94.8	5.107
^{52}Cr	3.31	1.471	0.925	1.0830	0.4440	3.539	304.1	4.466	99.3	5.068

Table B5

Results with the parameter $\lambda_2 = (1 + \lambda_1)/2$ fixed and parameter γ optimized.

Target	χ^2/F	γ (fm^2)	λ	c_m (fm)	a_m (fm)	$\langle r^2_m \rangle^{1/2}$ (fm)	$-J_v/4A$ (MeV fm^3)	$\langle r^2_v \rangle^{1/2}$ (fm)	$-J_w/4A$ (MeV fm^3)	$\langle r^2_w \rangle^{1/2}$ (fm)
^{40}Ca	2.80	1.645	1.000	1.0709	0.4900	3.371	320.1	4.344	102.6	4.901
^{42}Ca	3.18	1.680	0.987	1.1464	0.4136	3.448	315.3	4.394	109.9	4.939
^{43}Ca	2.42	1.569	0.975	1.0891	0.4830	3.458	316.9	4.399	106.0	4.975
^{44}Ca	3.31	1.670	0.983	1.1385	0.4159	3.476	312.6	4.421	113.2	4.964
^{48}Ca	3.26	1.568	1.000	1.0537	0.5186	3.537	320.6	4.484	96.2	5.104
^{50}Ti	1.88	1.574	0.968	1.1476	0.3876	3.578	310.5	4.492	96.5	5.043
^{51}V	2.47	1.539	0.971	1.1884	0.3694	3.680	317.6	4.557	95.7	5.096
^{52}Cr	1.62	1.573	0.963	1.0695	0.4569	3.528	302.6	4.481	98.3	5.073

Appendix C

Suppression of negative densities

In the folding model analyses the occurence of negative densities was reduced by introducing the constraint (eq. 13) into the analyses. How this constraint influences the results becomes obvious when comparing corresponding fits with and without the constraint. The example ^{40}Ca was chosen for this comparison yielding the results quoted in Table C 1

Table C 1 Occurence of negative densities with and without constraint (eq. 13)

Constraint	ν	μ	A^-_{max}
Without	12	4	-0.055
With	12	3	-0.022

ν Number of fits with different (but corresponding) values of N', R'_c

μ Number of fits with negative densities

A^-_{max} Maximum value of $A^- = A - \int |\rho_m(\vec{r})| d\vec{r}$

The comparison shows that also without constraint the number of cases with negative densities and the amount of negative densities is small. The reduction of such cases by the constraint (eq. 13) is - nevertheless - remarkable.

Appendix D

Numerical values of the extracted nuclear matter densities and corresponding errors of the even mass nuclei

NUCLEAR MATTER DENSITIES FROM ELASTIC ALPHA PARTICLE SCATTERING

TARGET	CA-40			CA-42		
RADIUS	DENSITY	ERROR	ERROR(%)	DENSITY	ERROR	ERROR(%)
0.0	2.3400E-01	3.7810E-02	16.16	1.5960E-01	3.8450E-02	24.09
0.1	2.3380E-01	3.7350E-02	15.98	1.5920E-01	3.7870E-02	23.79
0.2	2.3300E-01	3.6000E-02	15.45	1.5810E-01	3.6170E-02	22.88
0.3	2.3180E-01	3.3920E-02	14.63	1.5640E-01	3.3530E-02	21.44
0.4	2.2990E-01	3.1330E-02	13.63	1.5420E-01	3.0180E-02	19.57
0.5	2.2740E-01	2.8470E-02	12.52	1.5180E-01	2.6430E-02	17.41
0.6	2.2430E-01	2.5570E-02	11.40	1.4930E-01	2.2630E-02	15.16
0.7	2.2040E-01	2.2790E-02	10.34	1.4700E-01	1.9070E-02	12.97
0.8	2.1590E-01	2.0210E-02	9.36	1.4490E-01	1.6040E-02	11.07
0.9	2.1060E-01	1.7850E-02	8.48	1.4330E-01	1.3690E-02	9.55
1.0	2.0470E-01	1.5710E-02	7.67	1.4210E-01	1.2040E-02	8.47
1.1	1.9830E-01	1.3780E-02	6.95	1.4140E-01	1.0970E-02	7.76
1.2	1.9150E-01	1.2080E-02	6.31	1.4120E-01	1.0300E-02	7.29
1.3	1.8460E-01	1.0650E-02	5.77	1.4130E-01	9.8240E-03	6.95
1.4	1.7780E-01	9.5300E-03	5.36	1.4160E-01	9.3980E-03	6.64
1.5	1.7130E-01	8.7710E-03	5.12	1.4220E-01	8.9450E-03	6.29
1.6	1.6530E-01	8.3360E-03	5.04	1.4280E-01	8.4570E-03	5.92
1.7	1.6010E-01	8.1220E-03	5.07	1.4350E-01	7.9540E-03	5.54
1.8	1.5570E-01	8.0330E-03	5.16	1.4410E-01	7.4810E-03	5.19
1.9	1.5220E-01	8.0160E-03	5.27	1.4470E-01	7.0800E-03	4.89
2.0	1.4960E-01	8.0310E-03	5.37	1.4520E-01	6.7730E-03	4.66
2.1	1.4790E-01	8.0360E-03	5.43	1.4560E-01	6.5620E-03	4.51
2.2	1.4680E-01	7.9860E-03	5.44	1.4590E-01	6.4220E-03	4.40
2.3	1.4600E-01	7.8500E-03	5.38	1.4600E-01	6.3160E-03	4.33
2.4	1.4540E-01	7.6060E-03	5.23	1.4580E-01	6.2080E-03	4.26
2.5	1.4460E-01	7.2500E-03	5.01	1.4540E-01	6.0640E-03	4.17
2.6	1.4330E-01	6.7890E-03	4.74	1.4450E-01	5.8640E-03	4.06
2.7	1.4120E-01	6.2540E-03	4.43	1.4330E-01	5.6030E-03	3.91
2.8	1.3820E-01	5.7020E-03	4.13	1.4140E-01	5.3040E-03	3.75
2.9	1.3420E-01	5.2110E-03	3.88	1.3900E-01	5.0050E-03	3.60
3.0	1.2910E-01	4.8580E-03	3.76	1.3580E-01	4.7410E-03	3.49
3.1	1.2300E-01	4.6940E-03	3.82	1.3200E-01	4.5550E-03	3.45
3.2	1.1610E-01	4.7340E-03	4.08	1.2740E-01	4.4970E-03	3.53
3.3	1.0840E-01	4.9560E-03	4.57	1.2200E-01	4.5850E-03	3.76
3.4	1.0030E-01	5.2820E-03	5.27	1.1570E-01	4.7660E-03	4.12
3.5	9.2070E-02	5.5920E-03	6.07	1.0880E-01	4.9650E-03	4.56
3.6	8.3840E-02	5.8000E-03	6.92	1.0130E-01	5.1340E-03	5.07
3.7	7.5870E-02	5.8610E-03	7.73	9.3240E-02	5.2270E-03	5.61
3.8	6.8330E-02	5.7540E-03	8.42	8.4780E-02	5.2000E-03	6.13
3.9	6.1320E-02	5.4850E-03	8.94	7.6110E-02	5.0360E-03	6.62
4.0	5.4890E-02	5.0790E-03	9.25	6.7430E-02	4.7390E-03	7.03
4.1	4.9010E-02	4.5750E-03	9.33	5.8940E-02	4.3410E-03	7.37
4.2	4.3650E-02	4.0160E-03	9.20	5.0810E-02	3.8880E-03	7.65
4.3	3.8710E-02	3.4480E-03	8.91	4.3210E-02	3.4260E-03	7.93
4.4	3.4120E-02	2.9140E-03	8.54	3.6240E-02	2.9760E-03	8.21
4.5	2.9800E-02	2.4490E-03	8.22	3.0000E-02	2.5520E-03	8.51
4.6	2.5700E-02	2.0810E-03	8.10	2.4520E-02	2.1770E-03	8.88
4.7	2.1820E-02	1.8170E-03	8.33	1.9830E-02	1.8800E-03	9.48
4.8	1.8160E-02	1.6460E-03	9.06	1.5890E-02	1.6730E-03	10.53
4.9	1.4750E-02	1.5310E-03	10.38	1.2660E-02	1.5340E-03	12.12
5.0	1.1670E-02	1.4360E-03	12.31	1.0080E-02	1.4240E-03	14.13

5.1	8.9530E-03	1.3400E-03	14.97	8.0690E-03	1.3120E-03	16.26
5.2	6.6460E-03	1.2300E-03	18.51	6.5280E-03	1.1830E-03	18.12
5.3	4.7730E-03	1.0980E-03	23.00	5.3660E-03	1.0350E-03	19.29
5.4	3.3320E-03	9.5040E-04	28.52	4.4910E-03	8.7740E-04	19.54
5.5	2.2960E-03	8.0110E-04	34.89	3.8220E-03	7.2560E-04	18.98
5.6	1.6150E-03	6.7040E-04	41.51	3.2880E-03	6.0460E-04	18.39
5.7	1.2200E-03	5.7320E-04	46.98	2.8360E-03	5.2270E-04	18.43
5.8	1.0340E-03	5.0920E-04	49.25	2.4310E-03	4.7320E-04	19.47
5.9	9.8210E-04	4.6710E-04	47.56	2.0510E-03	4.4790E-04	21.84
6.0	9.9490E-04	4.3710E-04	43.93	1.6900E-03	4.3620E-04	25.81
6.1	1.0180E-03	4.0960E-04	40.24	1.3490E-03	4.1900E-04	31.06
6.2	1.0170E-03	3.7680E-04	37.05	1.0340E-03	3.8900E-04	37.62
6.3	9.7190E-04	3.3630E-04	34.60	7.5240E-04	3.4970E-04	46.48
6.4	8.8560E-04	2.9090E-04	32.85	5.1190E-04	3.0410E-04	59.41
6.5	7.7660E-04	2.4050E-04	30.97	3.1580E-04	2.4630E-04	77.99
6.6	6.5980E-04	2.2270E-04	33.75	2.3120E-04	2.1580E-04	93.34
6.7	5.3040E-04	1.9550E-04	36.86	1.7760E-04	1.8630E-04	104.90
6.8	3.9620E-04	1.6260E-04	41.04	1.3260E-04	1.6510E-04	124.51
6.9	2.7390E-04	1.2710E-04	46.40	1.1090E-04	1.4350E-04	129.40
7.0	1.7980E-04	8.7350E-05	48.58	1.3240E-04	1.1370E-04	85.88
7.1	1.3690E-04	8.5330E-05	62.33	1.1360E-04	1.1440E-04	100.70
7.2	1.0850E-04	7.4550E-05	68.71	9.1160E-05	1.0130E-04	111.12
7.3	8.6370E-05	5.5100E-05	63.80	6.6370E-05	7.5370E-05	113.56
7.4	6.6100E-05	2.9120E-05	44.05	4.2900E-05	3.9940E-05	93.10
7.5	6.5530E-05	CUT-OFF		4.3930E-05	CUT-OFF	
7.6	5.3440E-05			3.5070E-05		
7.7	4.3570E-05			2.8000E-05		
7.8	3.5530E-05			2.2350E-05		
7.9	2.8970E-05			1.7850E-05		
8.0	2.3630E-05			1.4250E-05		
8.1	1.9270E-05			1.1370E-05		
8.2	1.5710E-05			9.0780E-06		
8.3	1.2810E-05			7.2470E-06		
8.4	1.0450E-05			5.7850E-06		
8.5	8.5170E-06			4.6180E-06		
8.6	6.9450E-06			3.6870E-06		
8.7	5.6630E-06			2.9440E-06		
8.8	4.6170E-06			2.3490E-06		
8.9	3.7650E-06			1.8760E-06		
9.0	3.0700E-06			1.4980E-06		
9.1	2.5040E-06			1.1950E-06		
9.2	2.0420E-06			9.5430E-07		
9.3	1.6650E-06			7.6180E-07		
9.4	1.3570E-06			6.0810E-07		
9.5	1.1070E-06			4.8540E-07		
9.6	9.0230E-07			3.8750E-07		
9.7	7.3580E-07			3.0940E-07		
9.8	5.9990E-07			2.4700E-07		
9.9	4.8920E-07			1.9710E-07		
10.0	3.9890E-07			1.5740E-07		

NUCLEAR MATTER DENSITIES FROM ELASTIC ALPHA PARTICLE SCATTERING

TARGET	CA-44			CA-48		
RADIUS	DENSITY	ERROR	ERROR(%)	DENSITY	ERROR	ERROR(%)
0.0	1.0500E-01	5.1170E-02	48.73	1.5050E-01	4.1870E-02	27.82
0.1	1.0520E-01	5.0450E-02	47.96	1.5080E-01	4.1650E-02	27.62
0.2	1.0570E-01	4.8330E-02	45.72	1.5170E-01	4.1000E-02	27.03
0.3	1.0650E-01	4.5020E-02	42.27	1.5310E-01	3.9960E-02	26.10
0.4	1.0780E-01	4.0810E-02	37.86	1.5500E-01	3.8560E-02	24.88
0.5	1.0950E-01	3.6100E-02	32.97	1.5740E-01	3.6860E-02	23.42
0.6	1.1160E-01	3.1260E-02	28.01	1.6030E-01	3.4940E-02	21.80
0.7	1.1430E-01	2.6700E-02	23.36	1.6350E-01	3.2870E-02	20.10
0.8	1.1750E-01	2.2670E-02	19.29	1.6690E-01	3.0720E-02	18.41
0.9	1.2110E-01	1.9310E-02	15.95	1.7060E-01	2.8560E-02	16.74
1.0	1.2520E-01	1.6630E-02	13.28	1.7430E-01	2.6450E-02	15.17
1.1	1.2960E-01	1.4590E-02	11.26	1.7790E-01	2.4410E-02	13.72
1.2	1.3430E-01	1.3110E-02	9.76	1.8130E-01	2.2480E-02	12.40
1.3	1.3900E-01	1.2050E-02	8.67	1.8450E-01	2.0650E-02	11.19
1.4	1.4370E-01	1.1260E-02	7.84	1.8720E-01	1.8910E-02	10.10
1.5	1.4830E-01	1.0590E-02	7.14	1.8940E-01	1.7260E-02	9.11
1.6	1.5260E-01	9.9590E-03	6.53	1.9100E-01	1.5700E-02	8.22
1.7	1.5650E-01	9.3260E-03	5.96	1.9190E-01	1.4210E-02	7.40
1.8	1.5980E-01	8.7280E-03	5.46	1.9200E-01	1.2820E-02	6.68
1.9	1.6240E-01	8.2130E-03	5.06	1.9140E-01	1.1520E-02	6.02
2.0	1.6430E-01	7.8230E-03	4.76	1.8990E-01	1.0330E-02	5.44
2.1	1.6540E-01	7.5490E-03	4.56	1.8760E-01	9.2290E-03	4.92
2.2	1.6550E-01	7.3370E-03	4.43	1.8460E-01	8.2290E-03	4.46
2.3	1.6470E-01	7.1250E-03	4.33	1.8090E-01	7.3310E-03	4.05
2.4	1.6300E-01	6.8850E-03	4.22	1.7660E-01	6.5520E-03	3.71
2.5	1.6040E-01	6.6200E-03	4.13	1.7170E-01	5.9300E-03	3.45
2.6	1.5700E-01	6.3540E-03	4.05	1.6630E-01	5.5450E-03	3.33
2.7	1.5280E-01	6.1030E-03	3.99	1.6050E-01	5.3660E-03	3.34
2.8	1.4790E-01	5.8690E-03	3.97	1.5430E-01	5.3120E-03	3.44
2.9	1.4250E-01	5.6640E-03	3.97	1.4790E-01	5.3360E-03	3.61
3.0	1.3680E-01	5.5160E-03	4.03	1.4110E-01	5.4040E-03	3.83
3.1	1.3070E-01	5.4340E-03	4.16	1.3420E-01	5.4960E-03	4.10
3.2	1.2450E-01	5.4260E-03	4.36	1.2700E-01	5.5970E-03	4.41
3.3	1.1810E-01	5.4970E-03	4.65	1.1970E-01	5.6880E-03	4.75
3.4	1.1160E-01	5.6200E-03	5.04	1.1220E-01	5.7420E-03	5.12
3.5	1.0500E-01	5.7400E-03	5.47	1.0460E-01	5.7360E-03	5.48
3.6	9.8200E-02	5.7950E-03	5.90	9.6970E-02	5.6580E-03	5.83
3.7	9.1280E-02	5.7300E-03	6.28	8.9340E-02	5.5070E-03	6.16
3.8	8.4200E-02	5.5240E-03	6.56	8.1770E-02	5.2870E-03	6.47
3.9	7.6980E-02	5.1900E-03	6.74	7.4340E-02	5.0030E-03	6.73
4.0	6.9690E-02	4.7900E-03	6.87	6.7130E-02	4.6580E-03	6.94
4.1	6.2410E-02	4.4070E-03	7.06	6.0220E-02	4.2590E-03	7.07
4.2	5.5230E-02	4.0990E-03	7.42	5.3650E-02	3.8160E-03	7.11
4.3	4.8280E-02	3.8600E-03	8.00	4.7480E-02	3.3460E-03	7.05
4.4	4.1650E-02	3.6290E-03	8.71	4.1760E-02	2.8680E-03	6.87
4.5	3.5450E-02	3.3510E-03	9.45	3.6480E-02	2.4050E-03	6.59
4.6	2.9740E-02	3.0070E-03	10.11	3.1680E-02	1.9870E-03	6.27
4.7	2.4590E-02	2.6120E-03	10.62	2.7340E-02	1.6510E-03	6.04
4.8	2.0050E-02	2.2070E-03	11.01	2.3450E-02	1.4230E-03	6.07
4.9	1.6120E-02	1.8340E-03	11.38	2.0000E-02	1.2890E-03	6.44
5.0	1.2800E-02	1.5250E-03	11.91	1.6970E-02	1.2010E-03	7.08

5.1	1.0060E-02	1.2950E-03	12.87	1.4320E-02	1.1250E-03	7.86
5.2	7.8530E-03	1.1430E-03	14.55	1.2020E-02	1.0480E-03	8.72
5.3	6.1190E-03	1.0450E-03	17.08	1.0060E-02	9.6340E-04	9.58
5.4	4.7840E-03	9.7180E-04	20.31	8.3810E-03	8.7120E-04	10.39
5.5	3.7720E-03	8.9830E-04	23.81	6.9630E-03	7.7550E-04	11.14
5.6	3.0100E-03	8.1480E-04	27.07	5.7700E-03	6.8180E-04	11.82
5.7	2.4320E-03	7.2600E-04	29.85	4.7700E-03	5.9820E-04	12.54
5.8	1.9860E-03	6.4350E-04	32.40	3.9340E-03	5.3730E-04	13.66
5.9	1.6290E-03	5.8110E-04	35.67	3.2330E-03	5.0510E-04	15.62
6.0	1.3330E-03	5.4330E-04	40.76	2.6470E-03	4.9230E-04	18.60
6.1	1.0790E-03	5.1090E-04	47.35	2.1550E-03	4.7840E-04	22.20
6.2	8.5830E-04	4.6790E-04	54.51	1.7440E-03	4.4700E-04	25.63
6.3	6.6530E-04	4.0770E-04	61.28	1.4020E-03	3.9770E-04	28.37
6.4	4.9890E-04	3.2840E-04	65.82	1.1210E-03	3.3880E-04	30.22
6.5	3.5900E-04	2.3820E-04	66.35	8.9600E-04	2.7600E-04	30.80
6.6	2.5510E-04	2.0290E-04	79.54	7.2180E-04	2.5660E-04	35.55
6.7	1.8450E-04	1.7850E-04	96.75	5.9010E-04	2.3380E-04	39.62
6.8	1.6080E-04	1.6640E-04	103.48	4.9320E-04	2.0830E-04	42.23
6.9	1.4960E-04	1.6510E-04	110.36	4.2360E-04	1.7950E-04	42.37
7.0	1.3600E-04	1.5520E-04	114.12	3.7460E-04	1.4540E-04	38.81
7.1	1.1370E-04	1.5600E-04	137.20	3.1260E-04	1.3000E-04	41.59
7.2	8.9900E-05	1.3750E-04	152.95	2.6300E-04	1.0620E-04	40.38
7.3	6.9060E-05	1.0190E-04	147.55	2.2360E-04	7.5000E-05	33.54
7.4	4.9540E-05	5.3840E-05	108.68	1.9240E-04	3.8610E-05	20.07
7.5	4.2780E-05	CUT-OFF		1.6810E-04	CUT-OFF	
7.6	3.4000E-05			1.3960E-04		
7.7	2.7030E-05			1.1590E-04		
7.8	2.1480E-05			9.6300E-05		
7.9	1.7070E-05			7.9960E-05		
8.0	1.3570E-05			6.6420E-05		
8.1	1.0780E-05			5.5170E-05		
8.2	8.5740E-06			4.5820E-05		
8.3	6.8150E-06			3.8070E-05		
8.4	5.4170E-06			3.1620E-05		
8.5	4.3060E-06			2.6270E-05		
8.6	3.4220E-06			2.1820E-05		
8.7	2.7210E-06			1.8130E-05		
8.8	2.1620E-06			1.5060E-05		
8.9	1.7190E-06			1.2510E-05		
9.0	1.3660E-06			1.0400E-05		
9.1	1.0850E-06			8.6370E-06		
9.2	8.6300E-07			7.1760E-06		
9.3	6.8590E-07			5.9630E-06		
9.4	5.4520E-07			4.9550E-06		
9.5	4.3340E-07			4.1170E-06		
9.6	3.4440E-07			3.4220E-06		
9.7	2.7370E-07			2.8440E-06		
9.8	2.1760E-07			2.3630E-06		
9.9	1.7300E-07			1.9640E-06		
10.0	1.3750E-07			1.6330E-06		

NUCLEAR MATTER DENSITIES FROM ELASTIC ALPHA PARTICLE SCATTERING

TARGET	TI-50			CR-52		
RADIUS	DENSITY	ERROR	ERROR(%)	DENSITY	ERROR	ERROR(%)
0.0	1.6800E-01	6.0300E-02	35.89	1.6260E-01	7.6130E-02	46.82
0.1	1.6750E-01	5.9530E-02	35.54	1.6110E-01	7.5030E-02	46.57
0.2	1.6610E-01	5.7290E-02	34.49	1.5680E-01	7.1850E-02	45.82
0.3	1.6380E-01	5.3810E-02	32.85	1.5020E-01	6.6890E-02	44.53
0.4	1.6100E-01	4.9420E-02	30.70	1.4240E-01	6.0650E-02	42.59
0.5	1.5790E-01	4.4510E-02	28.19	1.3420E-01	5.3740E-02	40.04
0.6	1.5490E-01	3.9500E-02	25.50	1.2690E-01	4.6800E-02	36.88
0.7	1.5210E-01	3.4710E-02	22.82	1.2140E-01	4.0450E-02	33.32
0.8	1.5010E-01	3.0400E-02	20.25	1.1850E-01	3.5090E-02	29.61
0.9	1.4880E-01	2.6690E-02	17.94	1.1860E-01	3.0890E-02	26.05
1.0	1.4860E-01	2.3610E-02	15.89	1.2190E-01	2.7740E-02	22.76
1.1	1.4930E-01	2.1110E-02	14.14	1.2790E-01	2.5380E-02	19.84
1.2	1.5090E-01	1.9100E-02	12.66	1.3620E-01	2.3500E-02	17.25
1.3	1.5320E-01	1.7500E-02	11.42	1.4590E-01	2.1830E-02	14.96
1.4	1.5600E-01	1.6210E-02	10.39	1.5590E-01	2.0260E-02	13.00
1.5	1.5900E-01	1.5130E-02	9.52	1.6550E-01	1.8740E-02	11.32
1.6	1.6170E-01	1.4160E-02	8.76	1.7370E-01	1.7300E-02	9.96
1.7	1.6400E-01	1.3250E-02	8.08	1.7980E-01	1.6030E-02	8.92
1.8	1.6550E-01	1.2360E-02	7.47	1.8370E-01	1.4940E-02	8.13
1.9	1.6610E-01	1.1490E-02	6.92	1.8500E-01	1.3950E-02	7.54
2.0	1.6570E-01	1.0640E-02	6.42	1.8410E-01	1.3030E-02	7.08
2.1	1.6420E-01	9.8150E-03	5.98	1.8140E-01	1.2110E-02	6.68
2.2	1.6180E-01	9.0330E-03	5.58	1.7730E-01	1.1190E-02	6.31
2.3	1.5870E-01	8.3400E-03	5.26	1.7240E-01	1.0330E-02	5.99
2.4	1.5520E-01	7.8380E-03	5.05	1.6730E-01	9.7030E-03	5.80
2.5	1.5140E-01	7.6410E-03	5.05	1.6250E-01	9.4760E-03	5.83
2.6	1.4770E-01	7.7810E-03	5.27	1.5820E-01	9.7040E-03	6.13
2.7	1.4430E-01	8.1910E-03	5.68	1.5480E-01	1.0270E-02	6.63
2.8	1.4130E-01	8.7480E-03	6.19	1.5220E-01	1.0950E-02	7.19
2.9	1.3880E-01	9.3030E-03	6.70	1.5010E-01	1.1510E-02	7.67
3.0	1.3680E-01	9.7230E-03	7.11	1.4850E-01	1.1790E-02	7.94
3.1	1.3510E-01	9.9220E-03	7.34	1.4680E-01	1.1750E-02	8.00
3.2	1.3340E-01	9.8840E-03	7.41	1.4490E-01	1.1400E-02	7.87
3.3	1.3160E-01	9.6400E-03	7.33	1.4220E-01	1.0880E-02	7.65
3.4	1.2930E-01	9.2300E-03	7.14	1.3860E-01	1.0310E-02	7.44
3.5	1.2620E-01	8.7040E-03	6.90	1.3380E-01	9.7380E-03	7.28
3.6	1.2210E-01	8.1460E-03	6.67	1.2770E-01	9.2190E-03	7.22
3.7	1.1670E-01	7.6490E-03	6.55	1.2040E-01	8.8170E-03	7.32
3.8	1.1020E-01	7.2750E-03	6.60	1.1170E-01	8.5090E-03	7.62
3.9	1.0240E-01	7.0270E-03	6.86	1.0220E-01	8.2060E-03	8.03
4.0	9.3550E-02	6.8460E-03	7.32	9.1920E-02	7.8350E-03	8.52
4.1	8.3960E-02	6.6520E-03	7.92	8.1300E-02	7.3780E-03	9.08
4.2	7.3940E-02	6.3960E-03	8.65	7.0700E-02	6.8490E-03	9.69
4.3	6.3880E-02	6.0340E-03	9.45	6.0460E-02	6.2760E-03	10.38
4.4	5.4120E-02	5.5320E-03	10.22	5.0850E-02	5.6510E-03	11.11
4.5	4.4960E-02	4.9030E-03	10.91	4.2130E-02	4.9690E-03	11.79
4.6	3.6650E-02	4.2000E-03	11.46	3.4440E-02	4.2530E-03	12.35
4.7	2.9330E-02	3.4990E-03	11.93	2.7840E-02	3.5560E-03	12.77
4.8	2.3090E-02	2.8790E-03	12.47	2.2340E-02	2.9510E-03	13.21
4.9	1.7920E-02	2.3910E-03	13.34	1.7880E-02	2.4910E-03	13.93
5.0	1.3780E-02	2.0580E-03	14.93	1.4370E-02	2.1640E-03	15.06

5.1	1.0570E-02	1.8570E-03	17.57	1.1650E-02	1.9270E-03	16.54
5.2	8.1720E-03	1.7280E-03	21.15	9.5890E-03	1.7500E-03	18.25
5.3	6.4420E-03	1.6010E-03	24.85	8.0430E-03	1.6080E-03	19.99
5.4	5.2430E-03	1.4440E-03	27.54	6.8720E-03	1.4690E-03	21.38
5.5	4.4390E-03	1.2570E-03	28.32	5.9600E-03	1.3180E-03	22.11
5.6	3.9060E-03	1.0580E-03	27.09	5.2130E-03	1.1510E-03	22.08
5.7	3.5380E-03	8.7490E-04	24.73	4.5640E-03	9.8220E-04	21.52
5.8	3.2480E-03	7.3340E-04	22.58	3.9700E-03	8.2870E-04	20.87
5.9	2.9740E-03	6.4690E-04	21.75	3.4110E-03	7.0440E-04	20.65
6.0	2.6760E-03	6.0730E-04	22.69	2.8790E-03	6.1090E-04	21.22
6.1	2.3340E-03	5.8720E-04	25.16	2.3790E-03	5.3980E-04	22.69
6.2	1.9480E-03	5.5830E-04	28.66	1.9180E-03	4.7900E-04	24.97
6.3	1.5330E-03	5.0470E-04	32.92	1.5040E-03	4.1670E-04	27.71
6.4	1.1120E-03	4.2350E-04	38.08	1.1430E-03	3.4580E-04	30.25
6.5	7.1310E-04	3.1950E-04	44.80	8.3460E-04	2.6590E-04	31.86
6.6	4.7900E-04	2.6600E-04	55.53	6.3800E-04	2.3870E-04	37.41
6.7	2.9580E-04	2.0500E-04	69.30	4.8590E-04	2.0550E-04	42.29
6.8	1.6430E-04	1.5220E-04	92.64	3.7170E-04	1.6840E-04	45.31
6.9	1.5220E-04	1.2030E-04	79.04	2.8780E-04	1.2890E-04	44.79
7.0	1.8210E-04	9.4070E-05	51.66	2.2560E-04	8.7200E-05	38.65
7.1	1.7330E-04	1.0120E-04	58.40	1.7920E-04	8.0280E-05	44.80
7.2	1.4870E-04	9.3630E-05	62.97	1.4310E-04	6.7760E-05	47.35
7.3	1.1140E-04	7.1520E-05	64.20	1.1460E-04	4.9160E-05	42.90
7.4	6.5720E-05	3.8460E-05	58.52	9.1920E-05	2.5740E-05	28.00
7.5	5.0220E-05	CUT-OFF		7.3780E-05	CUT-OFF	
7.6	3.9640E-05			5.9030E-05		
7.7	3.1300E-05			4.7230E-05		
7.8	2.4720E-05			3.7790E-05		
7.9	1.9510E-05			3.0240E-05		
8.0	1.5410E-05			2.4190E-05		
8.1	1.2170E-05			1.9360E-05		
8.2	9.6030E-06			1.5490E-05		
8.3	7.5820E-06			1.2390E-05		
8.4	5.9870E-06			9.9130E-06		
8.5	4.7270E-06			7.9310E-06		
8.6	3.7320E-06			6.3450E-06		
8.7	2.9460E-06			5.0770E-06		
8.8	2.3260E-06			4.0620E-06		
8.9	1.8360E-06			3.2500E-06		
9.0	1.4500E-06			2.6000E-06		
9.1	1.1450E-06			2.0800E-06		
9.2	9.0370E-07			1.6640E-06		
9.3	7.1350E-07			1.3310E-06		
9.4	5.6330E-07			1.0650E-06		
9.5	4.4470E-07			8.5230E-07		
9.6	3.5110E-07			6.8190E-07		
9.7	2.7720E-07			5.4560E-07		
9.8	2.1880E-07			4.3650E-07		
9.9	1.7270E-07			3.4920E-07		
10.0	1.3640E-07			2.7940E-07		

Appendix E

Differential cross sections for ^{43}Ca, ^{51}V

SCATTERING OF 4-HE PARTICLES ON 43-CA

ELAB = 104.000 MEV Q = 0.0 MEV I = 7/2

ECM = 95.136 MEV K = 4.0827/FERMI ETA = 1.23581

LABORATORY DATA THETA DEGREE	SIGMA MB/SR	DSIGMA %	RUTHERFORD SIGMA/SR	CM DATA THETA DEGREE	SIGMA MB/SR	DSIGMA MB/SR
2.55	5.424E+05	10.2	6.967E-01	2.79	4.520E+05	4.590E+04
3.05	2.790E+05	15.0	7.333E-01	3.34	2.325E+05	3.484E+04
3.55	1.433E+05	13.8	6.914E-01	3.89	1.195E+05	1.652E+04
4.05	9.172E+04	9.2	7.493E-01	4.44	7.646E+04	7.045E+03
4.55	6.516E+04	8.3	8.478E-01	4.98	5.432E+04	4.517E+03
5.05	4.211E+04	10.2	8.312E-01	5.53	3.511E+04	3.597E+03
5.55	2.516E+04	12.1	7.242E-01	6.08	2.098E+04	2.536E+03
6.05	1.389E+04	15.4	5.643E-01	6.63	1.158E+04	1.782E+03
6.55	5.498E+03	22.4	3.068E-01	7.17	4.586E+03	1.028E+03
7.05	2.697E+03	21.0	2.019E-01	7.72	2.250E+03	4.722E+02
7.30	1.589E+03	23.7	1.367E-01	8.00	1.326E+03	3.146E+02
7.55	9.821E+02	14.8	9.669E-02	8.27	8.195E+02	1.213E+02
7.80	9.288E+02	4.1	1.042E-01	8.54	7.752E+02	3.204E+01
8.05	8.519E+02	6.3	1.084E-01	8.82	7.111E+02	4.496E+01
8.55	1.187E+03	7.2	1.921E-01	9.36	9.912E+02	7.142E+01
8.80	1.413E+03	6.6	2.564E-01	9.64	1.180E+03	7.837E+01
9.05	1.602E+03	3.7	3.253E-01	9.91	1.338E+03	4.903E+01
9.30	1.632E+03	3.7	3.694E-01	10.18	1.363E+03	5.072E+01
9.55	1.861E+03	4.6	4.682E-01	10.46	1.555E+03	7.106E+01
9.80	1.769E+03	1.3	4.933E-01	10.73	1.478E+03	1.902E+01
10.05	1.779E+03	2.6	5.486E-01	11.01	1.486E+03	3.929E+01
10.30	1.667E+03	3.3	5.670E-01	11.28	1.393E+03	4.586E+01
10.55	1.517E+03	3.3	5.679E-01	11.55	1.268E+03	4.180E+01
10.80	1.454E+03	5.6	5.975E-01	11.83	1.215E+03	6.791E+01
11.05	1.137E+03	7.3	5.120E-01	12.10	9.506E+02	6.986E+01
11.30	1.090E+03	6.6	5.367E-01	12.37	9.116E+02	6.024E+01
11.55	8.241E+02	12.3	4.427E-01	12.65	6.892E+02	8.496E+01
11.80	6.200E+02	14.1	3.627E-01	12.92	5.185E+02	7.323E+01
12.05	4.212E+02	16.9	2.679E-01	13.19	3.524E+02	5.951E+01
12.30	2.944E+02	18.6	2.032E-01	13.47	2.463E+02	4.580E+01
12.55	1.739E+02	25.9	1.301E-01	13.74	1.455E+02	3.764E+01
12.80	8.943E+01	32.2	7.234E-02	14.01	7.485E+01	2.409E+01
13.05	4.287E+01	39.1	3.746E-02	14.29	3.589E+01	1.404E+01
13.30	1.492E+01	60.9	1.406E-02	14.56	1.249E+01	7.600E+00
13.55	2.270E+00	181.6	2.304E-03	14.83	1.901E+00	3.452E+00
13.80	5.703E+00	79.5	6.225E-03	15.11	4.777E+00	3.796E+00
14.05	2.159E+01	45.6	2.531E-02	15.38	1.809E+01	8.246E+00
14.30	5.105E+01	28.2	6.420E-02	15.65	4.278E+01	1.207E+01
14.55	8.779E+01	17.6	1.183E-01	15.93	7.358E+01	1.293E+01
14.80	1.226E+02	13.0	1.768E-01	16.20	1.028E+02	1.338E+01
15.05	1.609E+02	7.2	2.480E-01	16.47	1.349E+02	9.756E+00
15.30	1.739E+02	5.2	2.861E-01	16.74	1.458E+02	7.597E+00
15.55	2.002E+02	4.3	3.514E-01	17.02	1.679E+02	7.280E+00
15.80	2.260E+02	3.7	4.499E-01	17.56	1.897E+02	7.052E+00
16.30	1.984E+02	3.3	4.199E-01	17.84	1.665E+02	5.446E+00
16.55	2.017E+02	1.8	4.535E-01	18.11	1.693E+02	2.967E+00
16.80	1.958E+02	4.5	4.672E-01	18.38	1.644E+02	7.426E+00
17.05	1.618E+02	7.0	4.094E-01	18.66	1.359E+02	9.579E+00
17.55	1.230E+02	6.0	3.491E-01	19.20	1.034E+02	6.247E+00
17.80	1.092E+02	6.9	3.279E-01	19.47	9.182E+01	6.353E+00
18.05	9.011E+01	9.9	2.859E-01	19.75	7.576E+01	7.533E+00
18.30	6.924E+01	12.3	2.320E-01	20.02	5.823E+01	7.152E+00
18.55	5.148E+01	13.5	1.820E-01	20.29	4.330E+01	5.850E+00
19.05	2.329E+01	17.9	9.149E-02	20.84	1.960E+01	3.498E+00
19.55	1.376E+01	8.8	5.989E-02	21.38	1.158E+01	1.023E+00
20.05	1.432E+01	5.7	6.890E-02	21.93	1.206E+01	6.876E-01
20.55	2.081E+01	10.9	1.104E-01	22.47	1.754E+01	1.906E+00
21.05	3.533E+01	6.8	2.061E-01	23.02	2.980E+01	2.028E+00
21.55	4.219E+01	4.2	2.701E-01	23.56	3.561E+01	1.500E+00
22.05	5.067E+01	2.6	3.551E-01	24.11	4.279E+01	1.108E+00
22.55	4.700E+01	1.9	3.599E-01	24.65	3.972E+01	7.654E-01
23.05	4.446E+01	2.4	3.712E-01	25.19	3.759E+01	8.874E-01
23.55	3.905E+01	3.8	3.549E-01	25.74	3.304E+01	1.253E+00
24.05	3.131E+01	5.6	3.090E-01	26.28	2.650E+01	1.489E+00
24.55	2.383E+01	6.5	2.552E-01	26.82	2.019E+01	1.313E+00
25.05	1.770E+01	6.9	2.052E-01	27.37	1.501E+01	1.031E+00
25.55	1.269E+01	6.3	1.590E-01	27.91	1.077E+01	6.827E-01
26.05	1.048E+01	4.7	1.417E-01	28.45	8.896E+00	4.188E-01
26.55	8.450E+00	4.0	1.231E-01	29.00	7.177E+00	2.867E-01

SCATTERING OF 4-HE PARTICLES ON 43-CA

LABORATORY DATA THETA DEGREE	SIGMA MB/SR	DSIGMA %	RUTHERFORD SIGMA/SR	CM DATA THETA DEGREE	SIGMA MB/SR	DSIGMA MB/SR
27.05	9.186E+00	2.2	1.440E-01	29.54	7.809E+00	1.740E-01
27.55	9.439E+00	2.4	1.590E-01	30.08	8.030E+00	1.967E-01
28.05	1.052E+01	2.1	1.901E-01	30.62	8.955E+00	1.906E-01
28.55	1.077E+01	1.8	2.087E-01	31.17	9.179E+00	1.654E-01
29.05	1.065E+01	1.8	2.208E-01	31.71	9.082E+00	1.600E-01
29.55	1.049E+01	2.4	2.325E-01	32.25	8.949E+00	2.170E-01
30.05	8.873E+00	3.5	2.100E-01	32.79	7.578E+00	2.648E-01
30.55	8.125E+00	3.4	2.051E-01	33.33	6.944E+00	2.384E-01
31.05	6.834E+00	4.0	1.838E-01	33.87	5.846E+00	2.314E-01
31.55	6.056E+00	4.5	1.734E-01	34.41	5.185E+00	2.308E-01
32.05	4.518E+00	7.0	1.375E-01	34.96	3.871E+00	2.706E-01
32.55	3.139E+00	5.7	1.015E-01	35.50	2.692E+00	1.540E-01
33.05	3.308E+00	2.2	1.135E-01	36.04	2.840E+00	6.361E-02
33.55	3.204E+00	3.1	1.165E-01	36.58	2.753E+00	8.618E-02
34.05	2.551E+00	5.9	9.826E-02	37.12	2.194E+00	1.302E-01
34.55	3.189E+00	3.1	1.300E-01	37.65	2.745E+00	8.496E-02
35.05	3.252E+00	2.1	1.401E-01	38.19	2.801E+00	5.882E-02
35.55	3.107E+00	2.8	1.414E-01	38.73	2.678E+00	7.413E-02
36.05	3.082E+00	2.3	1.481E-01	39.27	2.660E+00	6.240E-02
36.55	3.096E+00	2.3	1.569E-01	39.81	2.675E+00	6.278E-02
37.05	2.794E+00	3.7	1.492E-01	40.35	2.416E+00	9.004E-02
37.55	2.666E+00	3.1	1.499E-01	40.89	2.307E+00	7.244E-02
38.05	2.371E+00	2.9	1.403E-01	41.42	2.054E+00	5.968E-02
38.55	2.186E+00	2.9	1.361E-01	41.96	1.896E+00	5.457E-02
39.05	1.971E+00	3.6	1.289E-01	42.50	1.711E+00	6.086E-02
39.55	1.900E+00	2.3	1.305E-01	43.04	1.651E+00	3.796E-02
40.05	1.829E+00	2.6	1.318E-01	43.57	1.591E+00	4.064E-02
40.55	1.705E+00	3.2	1.289E-01	44.11	1.485E+00	4.751E-02
41.05	1.697E+00	2.0	1.344E-01	44.65	1.479E+00	3.016E-02
41.55	1.606E+00	2.4	1.407E-01	45.18	1.480E+00	3.556E-02
42.05	1.643E+00	3.4	1.427E-01	45.72	1.435E+00	4.949E-02
42.55	1.614E+00	2.4	1.466E-01	46.25	1.412E+00	3.404E-02
43.05	1.635E+00	2.7	1.553E-01	46.79	1.432E+00	3.899E-02
43.55	1.751E+00	6.9	1.739E-01	47.32	1.535E+00	1.056E-01
44.05	1.753E+00	2.3	1.817E-01	47.86	1.538E+00	3.550E-02
44.55	1.709E+00	2.5	1.849E-01	48.39	1.501E+00	3.769E-02
45.05	1.506E+00	7.3	1.700E-01	48.92	1.324E+00	9.612E-02
45.55	1.668E+00	2.9	1.964E-01	49.46	1.469E+00	4.279E-02
46.05	1.539E+00	3.1	1.880E-01	49.99	1.357E+00	4.243E-02
46.55	1.317E+00	7.2	1.683E-01	50.52	1.162E+00	8.390E-02
47.05	1.220E+00	3.1	1.623E-01	51.06	1.078E+00	3.390E-02
47.55	1.150E+00	2.6	1.592E-01	51.59	1.017E+00	2.651E-02
48.05	1.118E+00	7.1	1.610E-01	52.12	9.899E-01	7.005E-02
48.55	1.083E+00	3.3	1.621E-01	52.65	9.599E-01	3.206E-02
49.05	9.481E-01	3.4	1.476E-01	53.18	8.418E-01	2.883E-02
49.55	1.002E+00	2.7	1.620E-01	53.72	8.908E-01	2.364E-02
50.05	1.008E+00	2.8	1.692E-01	54.25	8.972E-01	2.536E-02
50.55	9.849E-01	2.6	1.716E-01	54.78	8.777E-01	2.325E-02
51.05	9.918E-01	2.7	1.793E-01	55.31	8.850E-01	2.421E-02
51.55	9.327E-01	3.4	1.748E-01	55.84	8.333E-01	2.801E-02
52.05	8.563E-01	3.6	1.664E-01	56.37	7.660E-01	2.751E-02
52.55	7.843E-01	3.4	1.579E-01	56.90	7.025E-01	2.404E-02
53.05	7.083E-01	3.4	1.477E-01	57.43	6.352E-01	2.166E-02
53.55	6.743E-01	3.8	1.465E-01	57.95	6.092E-01	2.294E-02
54.05	6.199E-01	3.4	1.385E-01	58.48	5.574E-01	1.898E-02
54.55	6.078E-01	3.5	1.406E-01	59.01	5.473E-01	1.941E-02
55.05	5.747E-01	4.1	1.375E-01	59.54	5.182E-01	2.136E-02
55.55	5.046E-01	4.8	1.248E-01	60.06	4.556E-01	2.179E-02
56.05	4.760E-01	4.6	1.217E-01	60.59	4.303E-01	1.965E-02
56.55	4.451E-01	3.5	1.175E-01	61.12	4.029E-01	1.414E-02
57.05	4.603E-01	4.7	1.277E-01	61.64	4.245E-01	1.988E-02
57.55	4.352E-01	5.3	1.225E-01	62.17	3.950E-01	2.080E-02
58.05	3.813E-01	4.9	1.114E-01	62.69	3.484E-01	1.716E-02
58.55	3.088E-01	5.6	9.262E-02	63.22	2.811E-01	1.561E-02
59.05	3.151E-01	5.3	9.749E-02	63.74	2.873E-01	1.520E-02
59.55	3.176E-01	4.2	1.013E-01	64.27	2.899E-01	1.221E-02
60.05	2.668E-01	5.9	8.772E-02	64.79	2.439E-01	1.442E-02
60.55	2.475E-01	6.5	8.387E-02	65.32	2.266E-01	1.484E-02
61.05	2.265E-01	5.5	7.906E-02	65.84	2.076E-01	1.146E-02
61.55	2.141E-01	4.0	7.697E-02	66.36	1.965E-01	7.932E-03
63.05	1.963E-01	4.7	7.697E-02	67.93	1.810E-01	8.514E-03
64.55	1.139E-01	6.3	4.858E-02	69.49	1.055E-01	6.593E-03
66.05	1.012E-01	5.9	4.684E-02	71.05	9.411E-02	5.545E-03
67.55	7.857E-02	6.0	3.939E-02	72.61	7.342E-02	4.439E-03
69.05	6.046E-02	6.7	3.275E-02	74.16	5.676E-02	3.782E-03
70.55	4.991E-02	6.9	2.914E-02	75.71	4.707E-02	3.245E-03
72.05	3.962E-02	8.7	2.489E-02	77.26	3.755E-02	3.263E-03
73.55	2.431E-02	9.0	1.640E-02	78.80	2.315E-02	2.075E-03
75.05	1.826E-02	9.7	1.320E-02	80.34	1.747E-02	1.698E-03
76.55	1.616E-02	11.2	1.250E-02	81.87	1.553E-02	1.738E-03
78.05	1.886E-02	9.5	1.557E-02	83.40	1.821E-02	1.726E-03

SCATTERING OF 4-HE PARTICLES ON 51-V

ELAB = 104.000 MEV Q = 0.0 MEV I = 7/2

ECM = 96.424 MEV K = 4.1380/FERMI ETA = 1.23581

LABORATORY DATA THETA DEGREE	SIGMA MB/SR	DSIGMA %	RUTHERFORD SIGMA/SR	CM DATA THETA DEGREE	SIGMA MB/SR	DSIGMA MB/SR
2.55	6.511E+05	8.4	8.358E-01	2.76	5.577E+05	4.708E+04
3.05	3.768E+05	12.4	9.899E-01	3.30	3.228E+05	4.012E+04
3.55	1.837E+05	14.4	8.854E-01	3.84	1.574E+05	2.271E+04
4.05	1.122E+05	9.4	9.161E-01	4.38	9.614E+04	8.991E+03
4.55	7.922E+04	7.9	1.030E+00	4.92	6.787E+04	5.359E+03
5.05	5.017E+04	9.7	9.897E-01	5.46	4.299E+04	4.170E+03
5.55	3.082E+04	11.3	8.866E-01	6.00	2.641E+04	2.984E+03
6.05	1.556E+04	14.9	6.318E-01	6.54	1.333E+04	1.985E+03
6.55	7.957E+03	15.7	4.438E-01	7.08	6.821E+03	1.070E+03
7.05	3.323E+03	20.9	2.487E-01	7.62	2.849E+03	5.941E+02
7.30	2.215E+03	15.8	1.905E-01	7.89	1.899E+03	2.992E+02
7.55	1.582E+03	11.5	1.557E-01	8.16	1.357E+03	1.557E+02
7.80	1.428E+03	3.2	1.600E-01	8.43	1.224E+03	3.860E+01
8.05	1.486E+03	5.6	1.889E-01	8.70	1.274E+03	7.101E+01
8.55	1.857E+03	7.1	3.003E-01	9.24	1.593E+03	1.124E+02
8.80	2.192E+03	4.3	3.977E-01	9.51	1.881E+03	8.006E+01
9.05	2.319E+03	3.3	4.706E-01	9.78	1.990E+03	6.551E+01
9.30	2.366E+03	1.2	5.352E-01	10.05	2.030E+03	2.431E+01
9.55	2.451E+03	2.8	6.163E-01	10.32	2.104E+03	5.903E+01
9.80	2.432E+03	2.1	6.779E-01	10.59	2.087E+03	4.309E+01
10.05	2.206E+03	3.1	6.799E-01	10.86	1.893E+03	5.925E+01
10.30	2.124E+03	3.7	7.222E-01	11.13	1.824E+03	6.774E+01
10.55	1.815E+03	4.6	6.789E-01	11.40	1.558E+03	7.208E+01
10.80	1.728E+03	6.3	7.099E-01	11.67	1.484E+03	9.311E+01
11.05	1.274E+03	8.6	5.733E-01	11.94	1.094E+03	9.409E+01
11.30	1.187E+03	7.4	5.840E-01	12.20	1.020E+03	7.572E+01
11.55	8.348E+02	15.3	4.481E-01	12.47	7.172E+02	1.095E+02
11.80	5.525E+02	17.6	3.230E-01	12.74	4.747E+02	8.356E+01
12.05	3.522E+02	19.3	2.239E-01	13.01	3.026E+02	5.830E+01
12.30	2.154E+02	20.7	1.486E-01	13.28	1.851E+02	3.836E+01
12.55	1.309E+02	26.5	9.786E-02	13.55	1.126E+02	2.988E+01
12.80	4.296E+01	54.1	3.474E-02	13.82	3.694E+01	1.997E+01
13.05	1.513E+01	49.7	1.321E-02	14.09	1.301E+01	6.459E+00
13.30	6.353E+00	61.2	5.983E-03	14.36	5.463E+00	3.341E+00
13.55	1.662E+01	37.0	1.686E-02	14.63	1.430E+01	5.286E+00
13.80	3.690E+01	30.3	4.026E-02	14.90	3.175E+01	9.616E+00
14.05	7.240E+01	23.0	8.482E-02	15.17	6.229E+01	1.435E+01
14.30	1.201E+02	17.7	1.509E-01	15.44	1.033E+02	1.832E+01
14.55	1.781E+02	11.5	2.399E-01	15.71	1.533E+02	1.769E+01
14.80	2.227E+02	7.0	3.210E-01	15.98	1.917E+02	1.344E+01
15.05	2.565E+02	4.2	3.935E-01	16.25	2.200E+02	9.227E+00
15.30	2.750E+02	2.6	4.522E-01	16.52	2.368E+02	6.252E+00
15.55	2.900E+02	1.5	5.086E-01	16.79	2.497E+02	3.672E+00
15.80	2.839E+02	2.2	5.647E-01	17.33	2.446E+02	5.261E+00
16.30	2.570E+02	4.3	5.435E-01	17.60	2.214E+02	9.434E+00
16.55	2.312E+02	4.2	5.195E-01	17.87	1.993E+02	8.407E+00
16.80	2.104E+02	4.5	5.017E-01	18.13	1.814E+02	8.188E+00
17.05	1.855E+02	7.2	4.690E-01	18.40	1.599E+02	1.149E+01
17.55	1.041E+02	10.6	2.954E-01	18.94	8.983E+01	9.552E+00
17.80	8.973E+01	9.3	2.692E-01	19.21	7.742E+01	7.185E+00
18.05	6.307E+01	15.0	2.000E-01	19.48	5.443E+01	8.160E+00
18.30	4.283E+01	16.0	1.434E-01	19.75	3.697E+01	5.901E+00
18.55	2.918E+01	16.2	1.031E-01	20.02	2.519E+01	4.084E+00
19.05	9.734E+00	23.6	3.822E-02	20.56	8.407E+00	1.988E+00
19.55	1.320E+01	13.7	5.743E-02	21.10	1.140E+01	1.559E+00
20.05	2.741E+01	12.0	1.318E-01	21.63	2.370E+01	2.848E+00
20.55	4.586E+01	7.5	2.431E-01	22.17	3.967E+01	2.995E+00
21.05	6.170E+01	4.3	3.597E-01	22.71	5.339E+01	2.291E+00
21.55	7.120E+01	1.7	4.555E-01	23.25	6.164E+01	1.034E+00
22.05	7.094E+01	1.7	4.969E-01	23.78	6.145E+01	1.040E+00
22.55	6.079E+01	3.2	4.652E-01	24.32	5.268E+01	1.689E+00
23.05	5.343E+01	4.1	4.459E-01	24.86	4.633E+01	1.880E+00
23.55	4.013E+01	6.9	3.645E-01	25.40	3.482E+01	2.396E+00
24.05	2.627E+01	7.8	2.592E-01	25.93	2.281E+01	1.788E+00
24.55	2.024E+01	6.4	2.165E-01	26.47	1.758E+01	1.118E+00

SCATTERING OF 4-HE PARTICLES ON 51-V

LABORATORY DATA THETA DEGREE	SIGMA MB/SR	DSIGMA %	RUTHERFORD SIGMA/SR	CM DATA THETA DEGREE	SIGMA MB/SR	DSIGMA MB/SR
25.05	1.394E+01	6.2	1.615E-01	27.01	1.212E+01	7.543E-01
25.55	1.200E+01	2.8	1.502E-01	27.54	1.043E+01	2.954E-01
26.05	1.252E+01	1.9	1.692E-01	28.08	1.089E+01	2.067E-01
26.55	1.304E+01	4.8	1.899E-01	28.61	1.135E+01	5.488E-01
27.05	1.850E+01	4.5	2.898E-01	29.15	1.612E+01	7.311E-01
27.55	2.092E+01	1.8	3.522E-01	29.69	1.824E+01	3.323E-01
28.05	2.067E+01	1.6	3.734E-01	30.22	1.803E+01	2.913E-01
28.55	1.869E+01	2.8	3.619E-01	30.76	1.631E+01	4.508E-01
29.05	1.640E+01	2.5	3.399E-01	31.29	1.433E+01	3.567E-01
29.55	1.542E+01	3.2	3.415E-01	31.83	1.347E+01	4.288E-01
30.05	1.200E+01	5.2	2.838E-01	32.36	1.049E+01	5.482E-01
30.55	9.607E+00	4.3	2.424E-01	32.90	8.407E+00	3.596E-01
31.05	8.343E+00	5.1	2.242E-01	33.43	7.306E+00	3.735E-01
31.55	5.643E+00	6.3	1.614E-01	33.97	4.945E+00	3.111E-01
32.05	4.910E+00	2.9	1.493E-01	34.50	4.306E+00	1.241E-01
32.55	4.512E+00	2.2	1.458E-01	35.03	3.960E+00	8.896E-02
33.05	4.633E+00	1.9	1.588E-01	35.57	4.069E+00	7.805E-02
33.55	4.850E+00	1.9	1.762E-01	36.10	4.263E+00	8.189E-02
34.05	5.033E+00	2.2	1.937E-01	36.64	4.427E+00	9.768E-02
34.55	4.598E+00	2.1	1.873E-01	37.17	4.048E+00	8.464E-02
35.05	4.535E+00	2.0	1.953E-01	37.70	3.995E+00	7.939E-02
35.55	4.216E+00	2.4	1.918E-01	38.23	3.717E+00	8.737E-02
36.05	4.003E+00	2.6	1.922E-01	38.77	3.532E+00	9.210E-02
36.55	3.522E+00	3.5	1.784E-01	39.30	3.110E+00	1.076E-01
37.05	3.015E+00	4.5	1.609E-01	39.83	2.665E+00	1.203E-01
37.55	2.353E+00	4.2	1.323E-01	40.36	2.082E+00	8.660E-02
38.05	2.179E+00	2.9	1.288E-01	40.90	1.929E+00	5.564E-02
38.55	1.905E+00	2.6	1.185E-01	41.43	1.688E+00	4.363E-02
39.05	1.903E+00	2.4	1.243E-01	41.96	1.687E+00	4.089E-02
39.55	1.957E+00	2.2	1.343E-01	42.49	1.737E+00	3.830E-02
40.05	2.012E+00	2.3	1.449E-01	43.02	1.787E+00	4.102E-02
40.55	1.871E+00	2.7	1.413E-01	43.55	1.664E+00	4.540E-02
41.05	1.964E+00	2.2	1.555E-01	44.08	1.748E+00	3.818E-02
41.55	1.971E+00	2.2	1.634E-01	44.61	1.756E+00	3.782E-02
42.05	2.067E+00	2.4	1.794E-01	45.14	1.843E+00	4.388E-02
42.55	2.090E+00	2.1	1.898E-01	45.67	1.865E+00	4.006E-02
43.05	1.997E+00	2.4	1.895E-01	46.20	1.783E+00	4.285E-02
43.55	1.847E+00	2.5	1.832E-01	46.73	1.651E+00	4.177E-02
44.05	1.725E+00	2.7	1.787E-01	47.26	1.544E+00	4.120E-02
44.55	1.580E+00	2.6	1.708E-01	47.79	1.415E+00	3.679E-02
45.05	1.620E+00	2.2	1.827E-01	48.32	1.452E+00	3.236E-02
45.55	1.590E+00	2.3	1.871E-01	48.85	1.427E+00	3.326E-02
46.05	1.528E+00	2.7	1.874E-01	49.37	1.373E+00	3.687E-02
46.55	1.403E+00	2.7	1.791E-01	49.90	1.261E+00	3.417E-02
47.05	1.450E+00	2.7	1.928E-01	50.43	1.305E+00	3.567E-02
47.55	1.305E+00	3.5	1.806E-01	50.96	1.176E+00	4.153E-02
48.05	1.487E+00	2.6	2.140E-01	51.48	1.341E+00	3.483E-02
48.55	1.487E+00	2.3	2.225E-01	52.01	1.343E+00	3.149E-02
49.05	1.474E+00	2.3	2.292E-01	52.54	1.332E+00	3.073E-02
49.55	1.455E+00	2.6	2.351E-01	53.06	1.317E+00	3.380E-02
50.05	1.310E+00	2.8	2.197E-01	53.59	1.186E+00	3.373E-02
50.55	1.268E+00	2.5	2.207E-01	54.12	1.149E+00	2.884E-02
51.05	1.247E+00	2.7	2.251E-01	54.64	1.131E+00	3.054E-02
51.55	1.145E+00	3.0	2.144E-01	55.17	1.040E+00	3.075E-02
52.05	1.172E+00	3.0	2.275E-01	55.69	1.066E+00	3.194E-02
52.55	1.035E+00	3.1	2.083E-01	56.22	9.428E-01	2.948E-02
53.05	1.016E+00	2.9	2.118E-01	56.74	9.264E-01	2.669E-02
53.55	9.673E-01	2.9	2.087E-01	57.26	8.828E-01	2.593E-02
54.05	9.543E-01	3.0	2.131E-01	57.79	8.718E-01	2.600E-02
54.55	8.603E-01	3.4	1.988E-01	58.31	7.869E-01	2.687E-02
55.05	8.339E-01	3.3	1.993E-01	58.83	7.636E-01	2.539E-02
55.55	8.637E-01	2.9	2.134E-01	59.36	7.917E-01	2.331E-02
56.05	8.270E-01	3.4	2.112E-01	59.88	7.590E-01	2.590E-02
56.55	7.572E-01	3.2	1.998E-01	60.40	6.958E-01	2.237E-02
57.05	7.515E-01	3.2	2.048E-01	60.92	6.913E-01	2.183E-02
57.55	7.236E-01	3.7	2.036E-01	61.45	6.664E-01	2.497E-02
58.05	6.370E-01	3.8	1.850E-01	61.97	5.873E-01	2.240E-02
58.55	6.155E-01	3.4	1.844E-01	62.49	5.661E-01	1.958E-02
59.05	5.965E-01	3.8	1.844E-01	63.01	5.513E-01	2.087E-02
59.55	5.437E-01	4.0	1.733E-01	63.53	5.031E-01	2.035E-02
60.05	4.853E-01	4.4	1.594E-01	64.05	4.495E-01	1.985E-02
60.55	4.575E-01	4.5	1.549E-01	64.57	4.244E-01	1.890E-02
61.05	4.368E-01	4.2	1.524E-01	65.09	4.056E-01	1.703E-02